JOURNAL OF GEOPHYSICAL RESEARCH, VOL. 114, A04102, doi:10.1029/2008JA013657, 2009

Multispacecraft recovery of a magnetic cloud and its origin from magnetic reconnection on the Sun

C. Möstl,[1,2] C. J. Farrugia,[3] C. Miklenic,[2] M. Temmer,[1] A. B. Galvin,[3] J. G. Luhmann,[4] E. K. J. Kilpua,[4,5] M. Leitner,[6] T. Nieves-Chinchilla,[7] A. Veronig,[1] and H. K. Biernat[1,2]

Received 31 July 2008; revised 25 November 2008; accepted 19 January 2009; published 10 April 2009.

[1] Multipoint spacecraft observations of a magnetic cloud on 22 May 2007 have given us the opportunity to apply a multispacecraft technique to infer the structure of this large-scale magnetic flux rope in the solar wind. Combining WIND and STEREO-B magnetic field and plasma measurements, we construct a combined magnetic field map by integrating the Grad-Shafranov equation, this being one of the very first applications of this technique in the interplanetary context. From this we obtain robust results on the shape of the cross section, the orientation and magnetic fluxes of the cloud. The only slightly "flattened" shape is discussed with respect to its heliospheric environment and theoretical expectations. We also relate these results to observations of the solar source region and its associated two-ribbon flare on 19 May 2007, using Hα images from the Kanzelhöhe observatory, SOHO/MDI magnetograms and SECCHI/EUVI 171 Å images. We find a close correspondence between the magnetic flux reconnected in the flare and the poloidal flux of the magnetic cloud. The axial flux of the cloud agrees with the prediction of a recent 3-D finite sheared arcade model to within a factor of 2, which is evidence for formation of at least half of the magnetic flux of the ejected flux rope during the eruption. We outline the relevance of this result to models of coronal mass ejection initiation, and find that to explain the solar and interplanetary observations elements from sheared arcade as well as erupting-flux-rope models are needed.

Citation: Möstl, C., et al. (2009), Multispacecraft recovery of a magnetic cloud and its origin from magnetic reconnection on the Sun, *J. Geophys. Res.*, *114*, A04102, doi:10.1029/2008JA013657.

1. Introduction

[2] The relative scarcity of interplanetary coronal mass ejections (ICMEs) in the first 1–2 years of STEREO operations has led to a concentration of effort on one or two events, most notably the ICME on 22 May 2007 [*Kilpua et al.*, 2009; *Liu et al.*, 2008] containing a magnetic cloud (MC [*Burlaga et al.*, 1981]). This has clear drawbacks because the event itself was not a particularly extraordinary ICME with its comparably weak magnetic field strength and low geo-effectiveness. It also had, however, unexpected benefits. One was that with the separation of STEREO-WIND of order the typical sizes of ICMEs, it has allowed a confirmation of their oblate nature directly from data [*Kilpua et al.*, 2009]. Another is that it has given us time to test various new techniques applicable to MCs. These will prove useful when more ejecta are seen as solar activity picks up.

[3] In this paper we make a further advance in the latter direction by using the Grad-Shafranov (GS) reconstruction technique [*Hau and Sonnerup*, 1999; *Hu and Sonnerup*, 2002] in a multispacecraft extension to get a more detailed view of the shape and to calculate global parameters such as axis orientation and magnetic fluxes to better accuracy. *Möstl et al.* [2008] have applied the multispacecraft methodology of *Sonnerup et al.* [2004] for the first time in an interplanetary context to simultaneous observations of a magnetic cloud made by WIND and ACE. There, the comparably small spacecraft separation ($\sim$400 R_E) essentially allowed a better estimate of the cloud's invariant axis and its shape in the vicinity of the spacecraft observations. In the 22 May 2007 event, the positions of the spacecraft STEREO A,B, WIND and ACE (roughly in the ecliptic and separated by 9.1° longitude) act together with the MCs inclined axis ($\sim$50–60° [*Kilpua et al.*, 2009]) to provide us with a unprecedented cut through a complete half of a MCs

[1]Institute of Physics, University of Graz, Graz, Austria.
[2]Space Research Institute, Austrian Academy of Sciences, Graz, Austria.
[3]Space Science Center and Department of Physics, University of New Hampshire, Durham, New Hampshire, USA.
[4]Space Sciences Laboratory, University of California, Berkeley, California, USA.
[5]Theoretical Physics Division, Department of Physics, University of Helsinki, Helsinki, Finland.
[6]Institute for Astro- and Particle Physics, University of Innsbruck, Innsbruck, Austria.
[7]Geospace Physics Laboratory, NASA Goddard Space Flight Center, Greenbelt, Maryland, USA.

0148-0227/09/2008JA013657$09.00

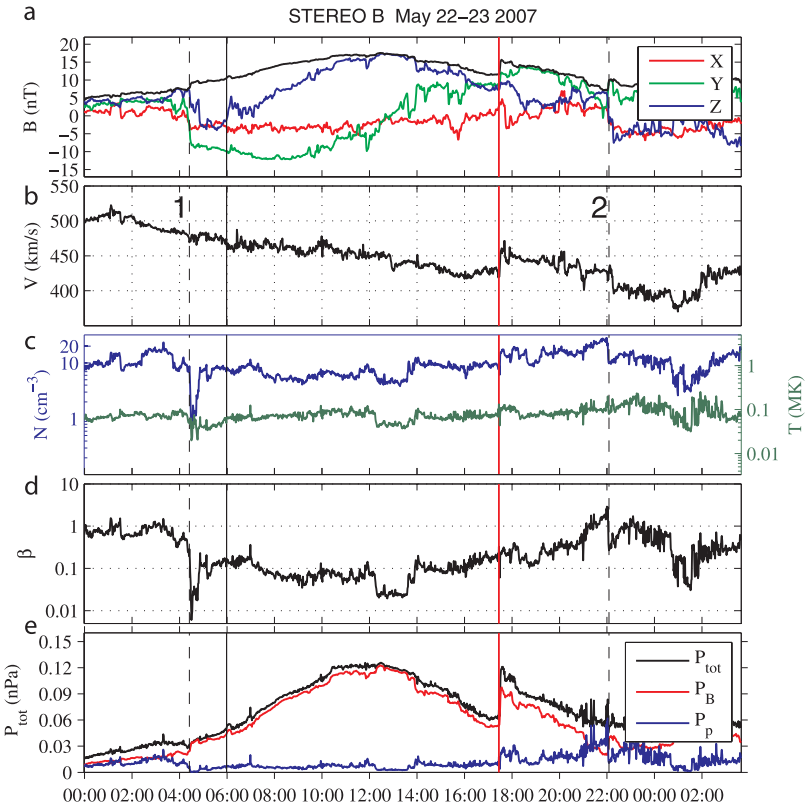

Figure 1. Magnetic field and plasma data (STEREO-B). The interval between the two solid lines is used for the reconstruction. The interval between dashed lines 1 and 2 is the MC interval determined from data [*Kilpua et al.*, 2009]. (a) Magnetic field magnitude and magnetic field components in cloud coordinates, (b) proton bulk velocity, (c) proton number density (blue) and proton temperature (green), (d) proton beta, and (e) total pressure (black) as the sum of magnetic (red) and proton pressure (blue).

cross section. This gives us the possibility to model the shape of a magnetic cloud for the first time and compare these results with the data-based inferences of *Kilpua et al.* [2009]. Note that the modeling of the complete 3-D configuration of a magnetic cloud in the heliosphere with its feet rooted to the Sun, or detached from it, is a future task which may be based on upcoming STEREO observations when these spacecraft are well separated in longitude, or future observations of ICME structure when multispacecraft observations closer to the Sun will be available.

[4] Our aims in this paper are twofold. First, we develop the methodology for creating a combined magnetic field map from the available magnetic cloud observations and discuss the results, especially the shape and magnetic fluxes. Secondly, the solar source region and the reconnected flux in its associated two-ribbon flare are discussed and compared to the resulting fluxes for the MC, in view of models of CME initiation.

[5] Magnetic clouds have been widely modeled as magnetic flux tubes with circular [e.g., *Burlaga*, 1988; *Lepping et al.*, 1990] or elliptical cross section [*Hidalgo et al.*, 2002; *Hidalgo*, 2003], as a torus [*Romashets and Vandas*, 2003; *Marubashi and Lepping*, 2007], or with an invariant direction but otherwise unconstrained geometry [e.g., *Hu and Sonnerup*, 2002; *Hu et al.*, 2004]. *Riley and Crooker* [2004] proposed from kinematic arguments that the extent of a MC in a plane perpendicular to its direction of motion could be very large (see also their Figure 1). In this case its shape should resemble a "pancake" with a larger lateral than radial dimension, which has been incorporated in the model of *Owens et al.* [2006]. Most of the above mentioned models presuppose a geometry, and thus the results of the single-spacecraft methods have to be viewed with some caution, especially for high impact parameters, as demonstrated by *Riley et al.* [2004], who applied some of these models to a numerical simulation.

[6] For the 22 May 2007 magnetic cloud, *Liu et al.* [2008] have found a good qualitative correspondence between the predictions of the single-spacecraft Grad-Shafranov (GS) modeling technique [*Hu and Sonnerup*, 2002] applied to STEREO-B observations and the corresponding magnetic field measurements by WIND and ACE, 0.06 AU away from STEREO-B. Based on this, the authors have estimated its aspect ratio to be at least 2:1, with an elongation perpendicular to its direction of motion. This is good evidence that (1) a magnetic cloud is well represented by the topology of a flux rope, and (2) that the assumptions of GS, especially time stationarity and $2\frac{1}{2}$ dimensionality, are well fulfilled, at least for this particular magnetic cloud at 1 AU. In contrast to *Liu et al.* [2008], we combine STEREO-B and WIND observations to produce a merged magnetic field map of the MC's cross section and quantitatively optimize the consistency between the predictions from the map and the actual observations.

[7] The second aim of this paper is to compare properties of the 22 May 2007 magnetic cloud as inferred from the multispacecraft technique to solar source observations of its associated two-ribbon flare in AR 958 on 19 May 2007 13:02 UT (GOES peak) [*Kilpua et al.*, 2009; *Li et al.*, 2008; see also *Miklenic et al.*, 2007]. The motivation for this comes from a recently found scaling between the reconnected magnetic fluxes in two-ribbon flares φ_r and the toroidal Φ_t and poloidal Φ_p magnetic fluxes in the corresponding magnetic clouds at Earth [*Longcope et al.*, 2007; *Qiu et al.*, 2007; *Möstl et al.*, 2008]. *Qiu et al.* [2007] studied nine events and found the relations $\Phi_p/\mathrm{AU} \approx \varphi_r$ and $\Phi_t \approx \varphi_r/3$. These results impose a constraint on CME initiation models and seem to favor the formation of the flux rope through magnetic reconnection of a sheared arcade, occurring in situ during the eruption process [e.g., *Moore and Labonte*, 1980; *Démoulin et al.*, 1996; *Antiochos et al.*, 1999; *Longcope and Beveridge*, 2007] (further called in situ models). In contrast to this, there are models where a preexisting flux rope erupts, either emerging completely through the photosphere [e.g., *Chen*, 1989; *Fan and Gibson*, 2007] or gradually being created there [e.g., *van Ballegooijen and Martens*, 1989]. We call both scenarios preexisting models. However, the transition between these two theories is not sharp, as pointed out by *Lin et al.* [2004], since the possibility exists that a preexisting flux rope erupts into the overlying coronal field and enhances its poloidal flux and mass through reconnection in its wake. In this later stage the same physical processes are at work as in the in situ models.

[8] A poorly know quantity is the length of the magnetic cloud flux tube from Sun to Earth, L. Estimates for this are in the range full length $L \approx 0.5-2$ AU at 1 AU. This puts an uncertainty factor of $\sim$4 in the measurement of the poloidal flux Φ_p (see discussions in the works of *Qiu et al.* [2007] and *Möstl et al.* [2008]), preventing a clear discrimination between the in situ and preexisting models. Owing to the lack of multispacecraft observations, the full cross section of a MC necessary for determining the axial flux Φ_t has not yet been recovered. In this paper we compare for the first time the more robust magnetic fluxes (especially the axial flux) of a multispacecraft modeled magnetic cloud with the associated flare reconnected flux, trying to avoid the large uncertainties connected to L and Φ_p. Our guideline in interpretation is thus not only (1) the 2-D standard flare model (preexisting: $\Phi_p > \varphi_r$, in situ: $\Phi_p \approx \varphi_r$) but also (2) the recent 3-D sheared arcade model by *Longcope and Beveridge* [2007] which predicts a relation between Φ_t and Φ_r depending on the shear, i.e., the distance by which the flare ribbons are displaced with respect to each other along the polarity inversion line. Changes of the shear during an eruption are known to be good indicators of the released magnetic energy [*Su et al.*, 2007].

[9] We start with a short discussion of the in situ observations at 1 AU in section 2. We then apply the multispacecraft technique in section 3. After an optimization procedure a merged magnetic field map is presented. How these results can be related to the solar source region with special emphasis on the magnetic fluxes in the ejecta and its associated two-ribbon flare are discussed in section 4, which is followed by the discussion section 5, where we discuss consequences of these results for the global configuration of magnetic clouds and for various CME-initiation models. Our conclusions are summarized in section 6.

2. In Situ Observations

[10] On 21–22 May 2007, the STEREO spacecraft pair and near-Earth spacecraft WIND and ACE encountered two ICMEs, with STEREO-B and WIND/ACE also clearly observing the signatures of a magnetic cloud in the first ICME [*Kilpua et al.*, 2009; *Liu et al.*, 2008]. The average spacecraft positions in GSE were $[-1056, 1344, -126]R_E$ for STEREO-B, $[1363, -2341, 26]R_E$ for STEREO-A and $[240, 91, 15]R_E$ for WIND (see Figure 1 in the work of *Kilpua et al.* [2009]). In Figures 1 and 2, magnetic field (in cloud coordinates) and plasma bulk parameters for STEREO-B and WIND are plotted. They were obtained from the IMPACT/MAG (magnetic field [*Acuña et al.*, 2007; *Luhmann et al.*, 2008]) and PLASTIC (plasma [*Galvin et al.*, 2008]) instruments aboard STEREO-B, and the MAG (magnetic field [*Lepping et al.*, 1995]) and SWE (plasma [*Ogilvie et al.*, 1995]) instruments aboard WIND. The time interval used for the reconstruction on STEREO-B is an outcome of the single-s/c technique and was determined to be 22 May 04:25 UT - 22 May 17:24 [*Kilpua et al.*, 2009]. Note that a shock-like discontinuity most probably driven by the trailing high-speed stream is penetrating into the back part of the cloud between WIND (at 1.01 AU) and STEREO-B (at 1.06 AU), which is a temporal rather than a spatial effect [*Kilpua et al.*, 2009].

3. Multispacecraft Grad-Shafranov Reconstruction in the Interplanetary Context

[11] In this section we discuss our approach to model the in situ observations by STEREO-B and WIND to produce a combined optimal magnetic field map of the MC orthogonal to the invariant axis determined by this method. For magnetic flux ropes, this "merging" approach has been used in the context of flux transfer events at the magnetopause [*Sonnerup et al.*, 2004; *Hasegawa et al.*, 2006] and for reconstructing a flux rope in the Earth's magnetotail [*Hasegawa et al.*, 2007]. Qualitative agreements between predictions of magnetic field maps from single-spacecraft GS and observations by other spacecraft have been shown by *Hu et al.* [2005] for magnetic clouds with spacecraft separations in the maps of 0.0014–0.0034 AU between WIND and ACE and for this event by *Liu et al.* [2008] for a separation between WIND and STEREO-B of 0.05 AU. For small spacecraft separation (0.0027 AU), the merging technique has been carried out for one case study [*Möstl et al.*, 2008]. In this paper we apply this method for the first time to observations in the interplanetary medium where the spacecraft separation distance is of the same order of magnitude as the size of the structure.

3.1. Elements of Grad-Shafranov Reconstruction

[12] Here we repeat some necessary basic elements of Grad-Shafranov reconstruction and highlight peculiarities in its use on magnetic clouds. The Grad-Shafranov (GS) technique [e.g., *Hau and Sonnerup*, 1999; *Hu and Sonnerup*, 2002; *Sonnerup et al.*, 2006] allows us to recover a $2\frac{1}{2}$ dimensional cross section of the MC magnetic structure in a plane perpendicular to an invariant axis $\hat{\mathbf{z}}$ by integrating

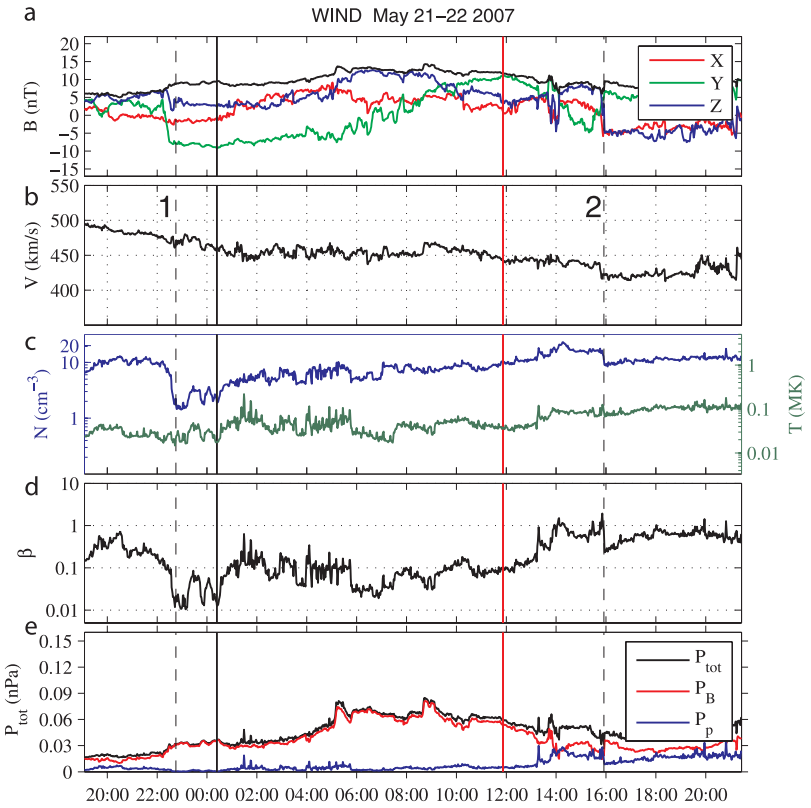

Figure 2. Magnetic field and plasma data (WIND, same format as Figure 1). The interval between the two solid lines is used for the reconstruction. The interval between dashed lines 1 and 2 is the MC interval determined from data [*Kilpua et al.*, 2009]. Note that the y axis in each subplot covers the same range as in Figure 1 for a direct comparison.

away from the spacecraft observations (trajectory) which are used as initial values, solving the Grad-Shafranov equation [*Sturrock*, 1994]. The GS method has its limitations: It treats the structure as magnetohydrostatic and thus time-independent ($d/dt = 0$) and presupposes the existence of an invariant direction ($\partial/\partial z = 0$), checked a posteriori. With respect to other techniques, GS has also distinct advantages, namely (1) no preconception on geometry, for example, a circular cross section, (2) it does not assume a force-free configuration and (3) it does not prescribe the number of flux tubes [see, e.g., *Hu et al.*, 2004].

[13] The reference frame moves with the structure with the deHoffmann-Teller velocity $\mathbf{V}_{HT}$ [*Khrabrov and Sonnerup*, 1998], i.e., the velocity for which the electric field $\mathbf{E} = (\mathbf{v} - \mathbf{V}_{HT}) \times \mathbf{B} \approx 0$. The intermediate variance direction obtained from minimum variance analysis (MVA [*Sonnerup and Cahill*, 1967]) is then taken as a preliminary guess of $\hat{\mathbf{z}}$. Subsequently, the original measurements are down-sampled with an anti-aliasing low-pass filter to a uniform grid with n_x points. Now, the single-spacecraft implementation of the technique uses the fact that the pressure transverse to the invariant direction $P_t(A) = p(A) + B_z^2(A)/8\pi$ must be single valued along a spacecraft trajectory to find the correct orientation of the invariant axis $\hat{\mathbf{z}}$ [*Hu and Sonnerup*, 2002]. Error bars on this orientation are usually in the range of ±10° [*Hu et al.*, 2004]. If multispacecraft measurements are available, this constraint can be augmented by searching for the highest correlation coefficients between predicted and observed field components [*Hasegawa et al.*, 2005]. For flux transfer events, *Hasegawa et al.* [2006] found the determination of $\hat{\mathbf{z}}$ from both methods to be within a few degrees if the model assumptions are approximately fulfilled. A cloud-centered coordinate system ($\hat{\mathbf{x}}$, $\hat{\mathbf{y}}$, $\hat{\mathbf{z}}$) is constructed, with $\hat{\mathbf{x}}$ being along the projected spacecraft trajectory onto the plane perpendicular to $\hat{\mathbf{z}}$ and $\hat{\mathbf{y}}$ completing the right handed triad [see *Hu and Sonnerup*, 2002]. Owing to time independence and constant $\mathbf{V}_{HT}$, time intervals can be directly converted into spatial distances with $dx = -\boldsymbol{V}_{HT} \cdot \hat{x}\, dt$. The vector potential A can then be calculated as

$$A(x,0) = -\int_0^x B_y(x',0)dx'. \tag{1}$$

From this and the observations follows the function $P_t(A)$ which is fitted by a polynomial with exponential tails. The Grad-Shafranov equation

$$\frac{\partial^2 A}{\partial x^2} + \frac{\partial^2 A}{\partial y^2} = -\mu_0 \frac{dP_t(A)}{dA} = -\mu_0 \frac{d\left(p + B_z^2/2\mu_0\right)}{dA}. \tag{2}$$

is then numerically solved to produce maps of $A(x, y)$ and $B_z(A(x, y))$ [*Hau and Sonnerup*, 1999]. The magnetic field is thus known everywhere in the domain and is represented by $\mathbf{B} = [\partial A(x, y)/\partial y, -\partial A(x, y)/\partial x, B_z(x, y)]$. Extrapolating functions are used in regions of the integration domain which are not covered by observations, commonly taken as

exponential functions. Note that only those field lines which are crossed twice by a spacecraft can be reconstructed reliably, as it is only for these that $P_t(A)$ can be checked for single valuedness.

[14] For magnetic clouds in the solar wind, *Hu and Sonnerup* [2002] and *Hu et al.* [2004, 2005] found that usually a deHoffmann-Teller (HT) frame with constant velocity can be very well determined and that $\mathbf{V}_{HT}$ is often very close to the radial direction pointing away from the Sun. Furthermore, residual velocities in the HT frame are small compared to the local Alfvén and acoustic speed (measured by the Walén slope w) and that the plasma pressure is often not a single-valued function of A alone. Thus one cannot construct maps of $p(A)$ for MCs. However, in these structures the magnetic pressure $B^2/2\mu_0$ dominates over the plasma pressure p (plasma $\beta \ll 1$) so the reconstruction method is still valid. Declining velocity profiles inside magnetic clouds are usually interpreted as signatures of radial expansion [e.g., *Klein and Burlaga*, 1982; *Farrugia et al.*, 1993]. This dynamic effect has not yet been included into the present technique. However, the expansion velocity V_{exp} can be calculated as $V_{\mathrm{exp}} = (V_l - V_t)/2$ with the leading edge (front boundary) velocity V_l and the trailing edge (back boundary) velocity V_t. The expansion effect is negligible if $V_{\mathrm{exp}}/V_{HT} \ll 1$. Whether it is so can be checked for a specific event.

[15] If a second spacecraft is nearby, the trajectory of this spacecraft can be projected onto the magnetic field map at a distance s_y, the latter being the y component of the separation vector $\mathbf{s} = \mathbf{p}_2 - \mathbf{p}_1$ between the positions $\mathbf{p}$ of spacecraft 1 and 2 projected into cloud coordinates. The corresponding time interval on the second spacecraft is calculated from assuming the cloud, and thus the box of the integration domain, moves with constant V_{HT} velocity. Thus this timeshift is given by

$$t = s_x/(\hat{\mathbf{x}} \cdot \mathbf{V}_{HT}) \tag{3}$$

i.e., the separation vector component s_x divided by the deHoffmann-Teller velocity along $\hat{\mathbf{x}}$.

3.2. Combining Observations Into a Composite Map

[16] We now proceed to merge the magnetic field maps provided by STEREO-B and WIND into a combined magnetic field map. This procedure has several advantages over the single-spacecraft method. These are (1) the consistency of the obtained maps from numerical integration with the observations of the other spacecraft can be checked with cross-correlation techniques, (2) parameters of the integration can be tuned to optimize this consistency, (3) the composite map is in better accordance with all the observations than any single-s/c map, (4) the spatial domain which can be covered by the integration of the GS equation is enlarged, thus mitigating one drawback of the method, and (5) inertia effects are included to a first-order approximation.

[17] We start with a time interval on STEREO-B of 22 May, 05:56 UT - 22 May, 17:24 and an initial invariant axis $\theta = 63°/\phi = 76°$ as derived from the single-s/c GS method [*Kilpua et al.*, 2009]. The initial separation to WIND is $\mathbf{s}_W = (0.0570, -0.0505, -0.0121)$ AU and the timeshift (equation (3)) is $t_W = -5.3$ h. Both quantities depend on the orientation and can be altered in the following iterative procedure.

[18] 1. A deHoffmann-Teller analysis [*Khrabrov and Sonnerup*, 1998] of the combined set of magnetic field and proton bulk velocity measurements during the respective cloud intervals is carried out. A correlation coefficent cc_{HT} between the components of $-\mathbf{v} \times \mathbf{B}$ and $-\mathbf{V}_{HT} \times \mathbf{B}$ is calculated as a measure of quality as well as a calculation of the Walén slope to estimate the role of dynamic effects. Note that for STEREO-B the plasma velocity was set to $V_x = -|V|$, $V_y = 0$, $V_z = 0$, i.e., assuming radial propagation, since components are not available.

[19] 2. A cloud coordinate system is constructed for a given invariant direction and the separation vector to WIND in GSE is projected into cloud coordinates to calculate $\mathbf{s}_W$ and the timeshift t. Step 1 is repeated for the new time interval.

[20] 3. The functions $P_t(A)$ (Figure 3) and $B_z(A)$ (not shown) are combined for both spacecraft and fitted by a polynomial of order f_p (solid black) with exponential tails (dashed black). For the WIND observations, a value of $A_g = 5$ T · m is added to A to better fit with the STEREO-B functions, this being equivalent to a gauge transformation [*Hasegawa et al.*, 2005]. A residue R_f as a measure of both the quality of the fit and the single-valued behavior of $P_t(A)$ and $B_z(A)$ is determined [*Hu et al.*, 2004].

[21] 4. From the combined $P_t(A)$ relation two individual magnetic field maps $A(x, y)$ from the STEREO-B and WIND observations are obtained by numerical integration on a 15×201 grid. Note that for the high impact parameter of WIND, guessing the extrapolating function (as would be the case in the single s/c method) is not necessary as the central parts of the MC are covered by STEREO-B observations. Two individual correlation coefficients cc_i are calculated between the observations and the predictions of the map at the trajectory of the respective other spacecraft not used for integration.

[22] 5. The two individual maps are merged into one composite map (Figure 4, grid size 15×251) by use of a Gaussian weighting function [*Sonnerup et al.*, 2004] with a width of 10% of the reconstruction domain ($d = 0.1$), a choice to be discussed below. Note that the integration domain covered by the STEREO-B map is not the same as for the WIND map, they are offset by a distance s_y. The low value of d is also necessary for a smooth transition at the edges of the maps.

[23] 6. A correlation coefficient cc of the observed magnetic field components and those predicted by the composite map (Figure 5) is calculated. Note that these predicted field components are partially merged with the observed ones and are not completely independent.

3.3. Optimization and Results

[24] We now proceed to tune parameters of the above procedure to simultaneously optimize the consistency given by cc_i while preserving the agreement with the model assumptions given by R_f. This is done by iterating the above points 1–6, so that these three parameters act as our guideline in searching for the best set of reconstruction parameters. In general, the correlation coefficients cc_i are a function of the orientation, the order of the fitting polynomial f_p, and the choice of the extrapolating functions f_e, i.e.,

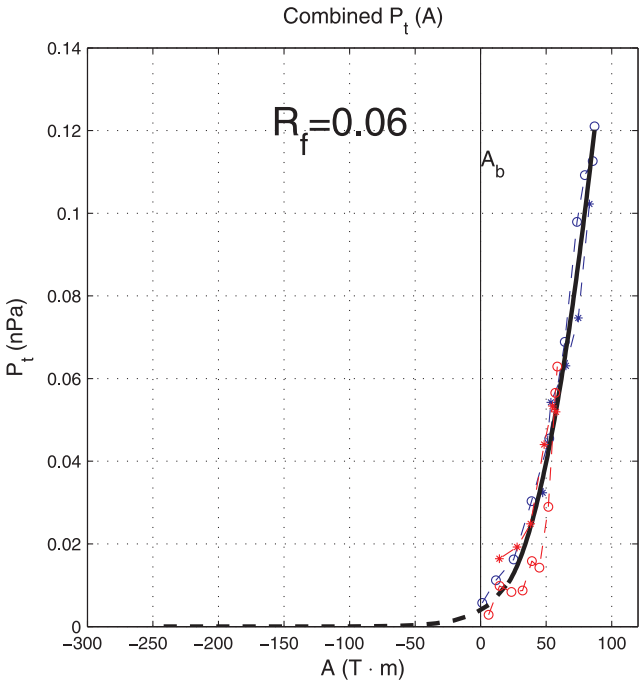

Figure 3. The transverse pressure $P_t(A)$ obtained from STEREO B observations (blue) and WIND (red) fitted by a third-order polynomial (solid black) and exponential tails (dashed black). The vertical line at a value of $A_b = 0$ corresponds to the white contour line in Figure 4.

$cc_i(\theta, \phi, f_p, f_e)$. We find cc_i to be most sensitive to the orientation angles θ and ϕ [cf. *Hasegawa et al.*, 2006] and generally highest for a value of $f_p = 2$. We keep the extrapolating functions fixed as exponentials as other choices do not improve cc_i. With $f_p = 2$ the fitting residue $R_f(\theta, \phi)$ as well as $cc_i(\theta, \phi)$ are functions of the orientation alone.

[25] We first searched for optimal angles (to be discussed below) and arrived at values of $\theta = 55 \pm 5°$ and $\phi = 70 \pm 10°$, with both $cc_i = 0.90$. In Figure 5, the magnetic field components in the combined map are correlated with the actual observations ($cc = 0.987$). The value of $R_f = 0.063$ is comparable to that found in other events studied in a single-spacecraft manner [*Hu and Sonnerup*, 2002; *Hu et al.*, 2005], demonstrating $P_t(A)$ to be approximately single-valued for both spacecraft. We note that the shape and magnetic fluxes are insensitive to an exact choice of these values. We emphasize that the correlation coefficients cc_i are not subject to any self-correlation, and the search for optimal angles was based on the constraint that high values of these two independent correlation coefficients should be accompanied by a low value of R_f, leading to the range of angles quoted above. For an orientation outside the range given, R_f became slightly higher but both cc_i became much lower. The coefficient cc (from the combined map) alone was not found to be very sensitive to the axis orientation.

[26] Concerning the HT analysis we find $\mathbf{V}_{HT} = [-450.5, 15.4, 9.0]$ km/s, a correlation coefficent $cc_{HT} = 0.9988$ between the components of $-\mathbf{v} \times \mathbf{B}$ and $-\mathbf{V}_{HT} \times \mathbf{B}$, and a Walén slope of $w = -0.045$, indicating that a good HT frame can be found and dynamic effects are negligible. The leading and trailing edge velocities at STEREO-B (WIND) are 473 (472) km/s and 429 (451) km/s, respectively. Taking the mean for each measurement, it follows that $V_{\exp} = 16$ km/s, and thus $V_{\exp}/|V_{HT}| = 0.036$ so the slight expansion does not significantly influence the results.

[27] We also varied the width of the Gaussian weight function. For decreasing d, cc rises but artifacts begin to show up for very low values of $d \approx 0.05$. For increasing $d \approx 0.2$, the map agrees less well with the observations since cc decreases. We find a reasonable compromise to be $d = 0.1$, which has the added advantage that the edges of the maps are sufficiently smoothed, because the two reconstruction domains for both spacecraft are not equal due to their large separation.

[28] Figure 4 shows the final combined magnetic field map, and Figure 6 shows a 3-D view of its helical field lines. The resulting somewhat oblate shape will be discussed in section 5.1. All final results are summarized in Table 1.

[29] The separation vector for STEREO-A with respect to STEREO-B in the combined field map is $\mathbf{s}_A = [0.1146 - 0.1336 - 0.0665]$ AU and $t_A = -10.7$ h. Thus the y separation in the map is a factor 2.5 larger than the y separation for WIND. In the combined magnetic field map (Figure 4), the time shifted observations are plotted as the bottom arrows. There exists an interval between arrows 3–

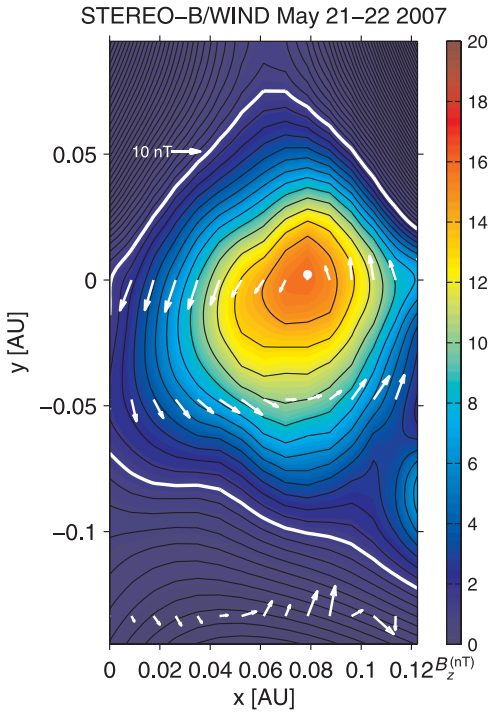

Figure 4. Combined magnetic field map reconstructed from STEREO B (top arrows) and WIND (middle arrows) for the interval ending at the shock. STEREO A observations are the bottom arrows. Black contour lines are transverse magnetic field lines. The B_z component, pointing out of the paper along the invariance direction, is color coded. White arrows are observed magnetic field components projected onto the x-y plane along the spacecraft trajectory.

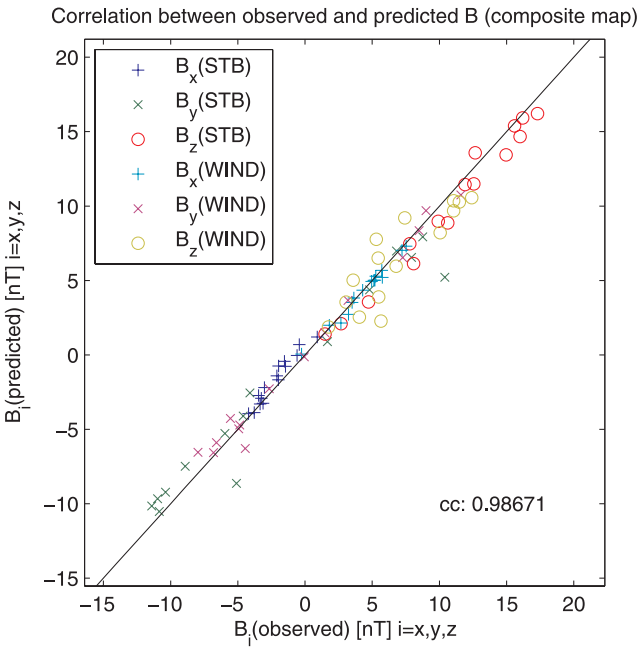

Figure 5. Comparison between predicted and observed magnetic field components in the combined magnetic field map. The symbol, e.g., B_x (STB) stands for a magnetic field x component in reconstruction coordinates observed at STEREO-B plotted against the prediction from the composite map.

11 (0.03–0.08 AU) including a smooth rotation of the field lines which is in good agreement with the rotation of the magnetic field at Wind and STEREO-B but not well modeled in the composite map. From the in situ magnetic field and plasma data plotted in Figure 7 one sees that the temperature and plasma β inside an interval of smoothly rotating field lines (21 May, 2200 UT - 22 May, 0100 UT, solid lines) are both low compared to the surrounding solar wind, satisfying the defining criteria for magnetic clouds. This 3-h-long interval is only 25% of the MC duration at STEREO-B, giving a further indication that, indeed, the MC flank is seen. At 0100 UT 22 May, a sharp peak in plasma β is seen, indicating the boundary between the cloud and the trailing high-speed stream.

[30] We also tried to include these STEREO-A observations into the combined magnetic field map but a single-valued function $P_t(A)$ could not be constructed. While from the magnetic field rotation and its short duration it seems quite likely that STEREO-A observes the far flank of the cloud, it cannot be included in a straightforward way in the present technique, probably because the MC's flank is strongly interacting with the surrounding solar wind. That the far flank of the MC is indeed seen by STEREO-A also indicates that its aspect ratio might not exceed much the value of 1.3:1 calculated from the ratio of twice its separation in the map (including the effect of orientation) to its full diameter (~0.25 AU/0.19 AU). This aspect ratio of 1.3:1 should be seen as a lower limit due to (1) the limited spatial domain covered by the reconstruction, and (2) the lack of observations beyond STEREO-A, but we emphasize that the MC interval is much shorter at STEREO-A than at the other two spacecraft closer to the axis, implying that an aspect ratio of larger than ≈1.5:1 is rather unlikely.

3.4. Magnetic Fluxes in the Cloud

[31] The poloidal magnetic flux is given by $\Phi_p = |A_b - A_m| L$ [*Qiu et al.*, 2007], with A_b denoting the cloud's outer boundary and A_m the value of the vector potential at the axis, determined at the maximum of $B_z(A)$ (white dot in Figure 4). As is seen from the field map, the axis is very close to the STEREO-B trajectory (impact parameter 0.0021 AU). The poloidal flux is found to be $\Phi_p = 1.24 \times 10^{21}$Mx/AU, and for a length of $L = 0.5–2$ AU, Φ_p varies between $0.62–2.48 \times 10^{21}$ Mx.

[32] The toroidal (axial) flux $\Phi_t = \int\int B_z\, dx\, dy$ inside A_b is 0.27×10^{21} Mx. This is a lower limit, because (1) the observations by STEREO-B and WIND cover mostly the lower half of the cross section (Figure 4) so that the extension of the cross section in the positive $\hat{\mathbf{y}}$ direction may be underestimated, (2) it is not possible to reconstruct field lines behind the shock on 22 May 17:24 (STEREO-B) because its presence violates the model assumptions, and (3) the STEREO-A observations of the MCs flank indicate that the true extension in $-\hat{\mathbf{y}}$ of the cloud is underestimated by the combined map.

[33] To compensate for (1) we estimate an upper boundary axial flux by calculating only the lower half of the cross

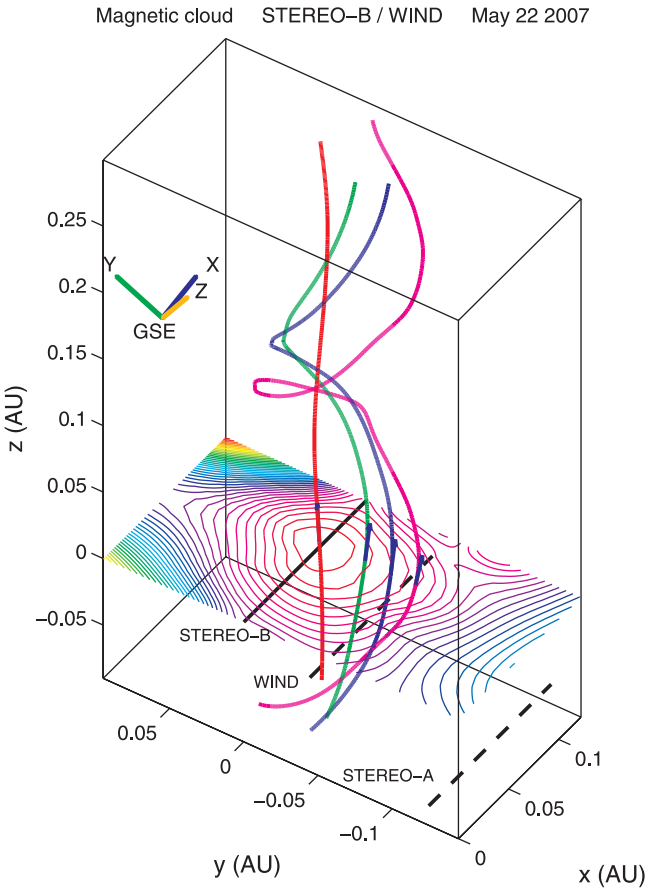

Figure 6. Three-dimensional view of the spiral magnetic cloud field lines. Spacecraft trajectories and the GSE unit vectors are indicated.

Table 1. Results of the Two-Spacecraft Grad-Shafranov Reconstruction[a]

	Results
STB interval	22 May 05:56 to 22 May 17:24
WIND interval	21 May 00:24 to 22 May 11:52
STA interval	21 May 18:52 to 22 May 06:20
$\mathbf{s}_W$ (AU)	[0.0585, −0.0475, −0.0165]
$\mathbf{s}_A$ (AU)	[0.1146, −0.1336, −0.0665]
$\mathbf{V}_{HT}$ (km/s)	(−450.3, 15.0, 8.8)
cc_{HT}	0.9988
w	−0.0443
R_f	0.0628
θ (deg) (GS, FF, MV, HM)	55 (63, 44, 53, 60)
ϕ (deg) (GS, FF, MV, HM)	75 (76, 99, 77, 123)
H (GS,FF, MV, HM)	R (R,R,R,R)
D (AU) (FF, MV)	0.123 (0.19, 0.19)
p_{STB} (AU) (FF, HM)	0.002 (0.004, 0.061)
B_0 (nT) (GS, FF, MV, HM)	16.2 (17.6, 18.5, 17, 24)
Φ_t (10^{21} Mx) (GS, FF)	0.33 ± 0.05 (0.21, 0.51 ± 0.18)
Φ_p (10^{21} Mx/AU) (GS, FF)	1.24 (0.82, 1.64 ± 0.37)

[a]Intervals are used for the observations (arrows) in Figure 4. Results of single-spacecraft methods applied to the STEREO-B data are in brackets. GS2, two-spacecraft Grad-Shafranov reconstruction; GS, Grad-Shafranov technique; FF, force-free fitting; MV, minimum variance analysis; HM, Hidalgo model. Intervals are 22 May 0430 UT to May 1730 UT for GS and HM; 22 May 0430 UT to 22 May 2200 for FF and MV.

section and multiplying this flux by 2, yielding $\Phi_t = 0.337 \times 10^{21}$ Mx. As determined by *Kilpua et al.* [2009], the cloud's back boundary can be set around 22:05, 22 May (STEREO-B), and thus the last ≈35% of the cloud are not covered by the reconstruction. To estimate how much axial flux is missed, in Figure 8 the magnetic fluxes for decreasing values of the boundary A_b are plotted [*Möstl et al.*, 2008], i.e., from inside out. This function becomes flat for low A_b, indicating that the outer parts of the cloud contribute only little to the axial flux so effects (2) and (3) may not significantly influence the final results. This was found for another MC [*Möstl et al.*, 2008], but the flattening is much more pronounced for this event because the combined map covers a larger area of the cloud. In summary, we estimate the toroidal flux from GS2 to be $\Phi_t = 0.33 \pm 0.05 \times 10^{21}$ Mx.

3.5. Comparison With Minimum Variance Analysis and Fitting Techniques

[34] In view of the results obtained in the last section, how much can we trust widely used single-spacecraft methods in determining global magnetic cloud parameters for a central crossing of the structure? The methods most widely used are minimum variance analysis and force-free fitting. For both of these methods we used the full cloud interval from 22 May 04:30 UT - May 22:00 UT as in principle both methods allow us to use this interval, in contrast to GS. Additionally, the *Hidalgo et al.* [2002]

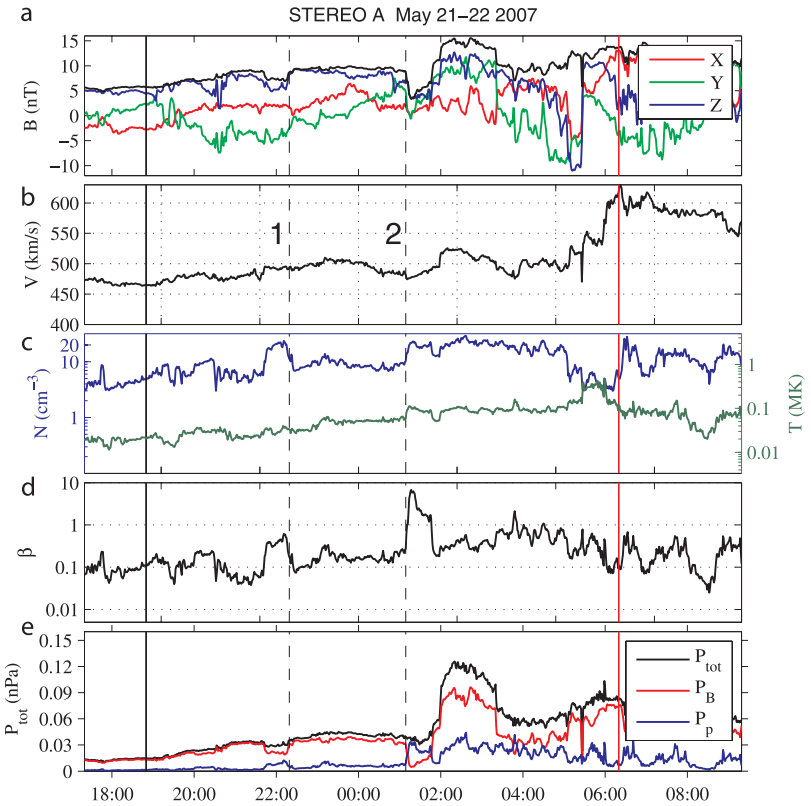

Figure 7. STEREO A magnetic field and plasma data (same format as Figure 1). The magnetic field is again rotated into reconstruction coordinates. Dashed lines 1 and 2 denote boundaries of the MC (equal to 0.03 to 0.07 AU along the x axis in Figure 4). The two solid lines indicate the full interval of vectors plotted in Figure 4. The y axis in Figures 7c–7e cover the same ranges as in Figures 1 and 2 for direct comparison.

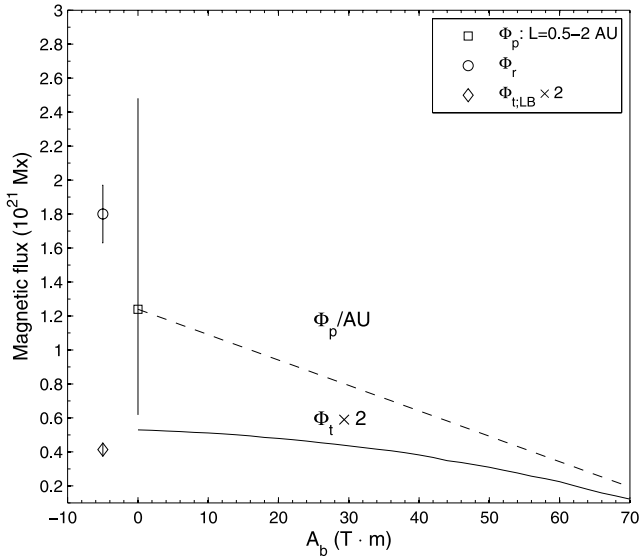

Figure 8. Cumulated magnetic fluxes in the MC, toroidal Φ_t (solid, multiplied by 2) and poloidal Φ_p (dashed) as function of the boundary of the vector potential A_b, from the inside (high A_b) to the outside (low A_b) of the flux rope. The range of Φ_p (square) is given with an uncertainty from L = 0.5–2 AU. The flare reconnected flux φ_r (circle) and the prediction of the axial flux $\Phi_{t;LB} = 0.1148\varphi_r$ (diamond, multiplied by 2) for S = 0.8 from the [*Longcope and Beveridge*, 2007] model are indicated.

model relaxes some of the assumptions of the force-free and circular cross-section flux rope model, allowing a nonforce free treatment including expansion and an elliptical cross section.

[35] The orientation angles obtained from applying minimum variance analysis (MV [e.g., *Sonnerup and Cahill*, 1967; *Huttunen et al.*, 2005]) to the STEREO-B observations are stated in brackets in Table 1. They are only 3° (θ) and 2° (ϕ) degrees away from the new method, indicating that for a very low impact parameter MV is in good agreement with GS2. Impact parameters and magnetic fluxes can only be derived in connection with the force-free Lundquist solution [*Gulisano et al.*, 2007].

[36] Applying the method of directly fitting this force-free solution to the magnetic field signatures of STEREO-B (FF method [e.g., *Burlaga*, 1988; *Lepping et al.*, 1990; *Lynch et al.*, 2005; *Leitner et al.*, 2007]) results in the fit shown in Figure 9. Apart from the total field strength, the variations of the magnetic field components are reasonably well modeled. The magnetic fluxes are given for example by equations (2) and (3) in the work of *Lynch et al.* [2005]. They depend on the central axial field strength B_0 and either on the cloud radius R_0 or the force-free parameter $\alpha = 2.4048/R_0$. The results are again stated in brackets in Table 1. The error bars were estimated by varying $B_0 = 18.5 \pm 2$ nT and $R_0 = 0.095 \pm 0.01$ AU, translating to an uncertainty in D of 0.02 AU. It follows that $\Phi_{t;FF} = 0.51 \pm 0.18 \times 10^{21}$ Mx and $\Phi_{p;FF} = 1.64 \pm 0.37 \times 10^{21}$ Mx/AU. Additionally, varying L = 0.5–2 AU results in a range of $\Phi_{p;FF} = 0.66 - 4.03 \times 10^{21}$ Mx. We also note that fitting the shorter interval gives B_0 = 20 nT and R_0 = 0.13 AU which yields $\Phi_{t;FF} = 0.26 \pm 0.12 \times 10^{21}$ Mx and $\Phi_{p;FF} = 1.22 \pm 0.33 \times 10^{21}$ Mx/AU. Both values are remarkably close to the values inferred from GS2.

[37] We also used the model of *Hidalgo et al.* [2002] (HM) to interpret the STEREO-B magnetic cloud signatures. The results are included in Table 1, using the shorter interval which yields a better fit. The aspect ratio of the ellipse is 1:2.2, being larger than that obtained from GS2 (1:1.3) assuming STEREO-A observes the flank of the cloud. The model gives a higher axial field strength (24 nT), a larger longitude (123°) as well as an higher impact parameter compared to the other methods.

[38] For completeness, Table 1 includes results from single-spacecraft GS. Angle θ is 13° higher than from the new method because behind the shock an interval of southward B_z was not included in its determination. The magnetic fluxes are both underestimates as the reconstruction interval of the MC stops at the shock and a smaller area was used; see Table 1 and Figure 6 in the work of *Kilpua et al.* [2009].

[39] In conclusion, we find the poloidal flux from force-free fitting in about the same range as the one inferred from GS2. The FF axial flux is about 50% larger compared to GS2, arising mostly from the larger radius. However, we note that GS2 and FF agree remarkably well on global cloud parameters for a spacecraft crossing close to the axis, which is likely a consequence of the central field lines possessing a close-to-circular shape (Figure 4). Combining the analysis by taking into account the larger radius and the results from FF, a reasonable estimate of the toroidal flux in the 22 May 2007 magnetic cloud is $\Phi_t = 0.4 \pm 0.1 \times 10^{21}$ Mx. Its uncertainty is less than a factor of 2 compared to Φ_p which has an uncertainty of at least a factor 4.

4. Solar Observations

[40] The aim of this section is (1) to determine the reconnected flux in the associated flare on 19 May 2007 13:00 UT in the western part of AR 10956 and relate the flare reconnected flux to the MC flux, and (2) to associate the structure of the active region surrounding the flare site to the magnetic cloud structure at 1 AU in terms of handedness and orientation. This eruption has been shown before to be the solar source of the 21–22 May 2007 magnetic cloud [*Kilpua et al.*, 2009] and we will also support this connection with height-time plots from LASCO and STEREO/COR1 observations. Figure 10 gives an overview of the event.

4.1. Flare Evolution and Reconnected Magnetic Flux

[41] The B9.5/SF flare event on 19 May 2007 (begin at ~12:47 UT, maximum at 13:02 UT) was located in NOAA Active Region 10956 near the center of the solar disk (N01W05). High-cadence (~60 s) full-disk imaging in the Hα spectral line provided by the Kanzelhöhe Solar Observatory (KSO, Austria [*Otruba and Pötzi*, 2003]) show two filament eruptions before and during the impulsive phase of the event, as well as two bright flare ribbons, separating from each other and from the polarity inversion line, as the flare progresses (see Figure 11). Five successive full-disk line-of-sight magnetograms 1-min apart, derived from the MDI instrument [*Scherrer et al.*, 1995] on board the Solar and Heliospheric Observatory (SOHO), were averaged

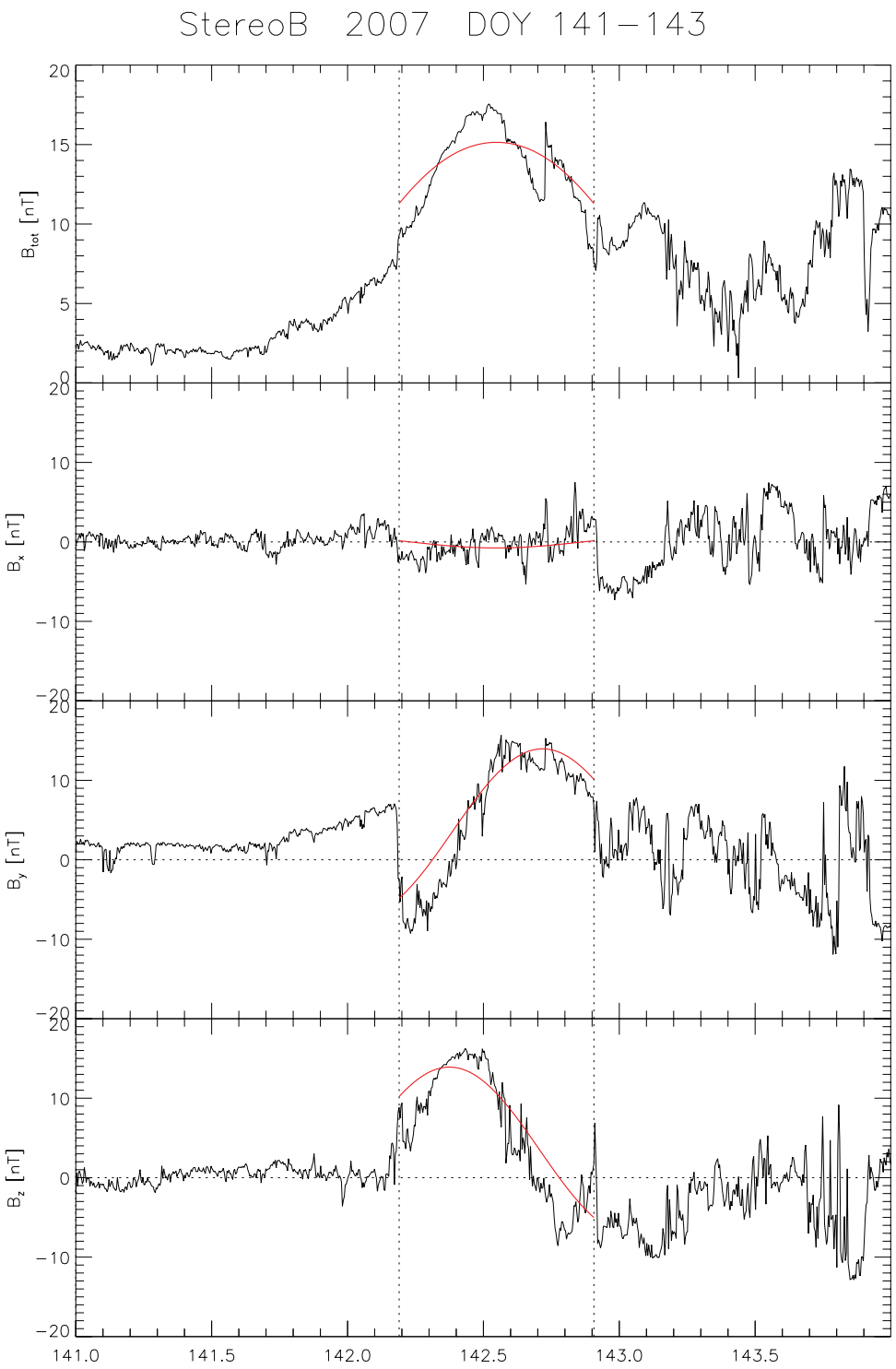

Figure 9. Force-free fitting of STEREO-B magnetic field data using the longer interval 22 May 0430 UT to 22 May 2200 UT. The rotation of the observed magnetic field components (GSE, black) is well fitted by a circular Lundquist flux rope (red) with orientation $\theta = 44°$; $\phi = 99°$ (see Table 1).

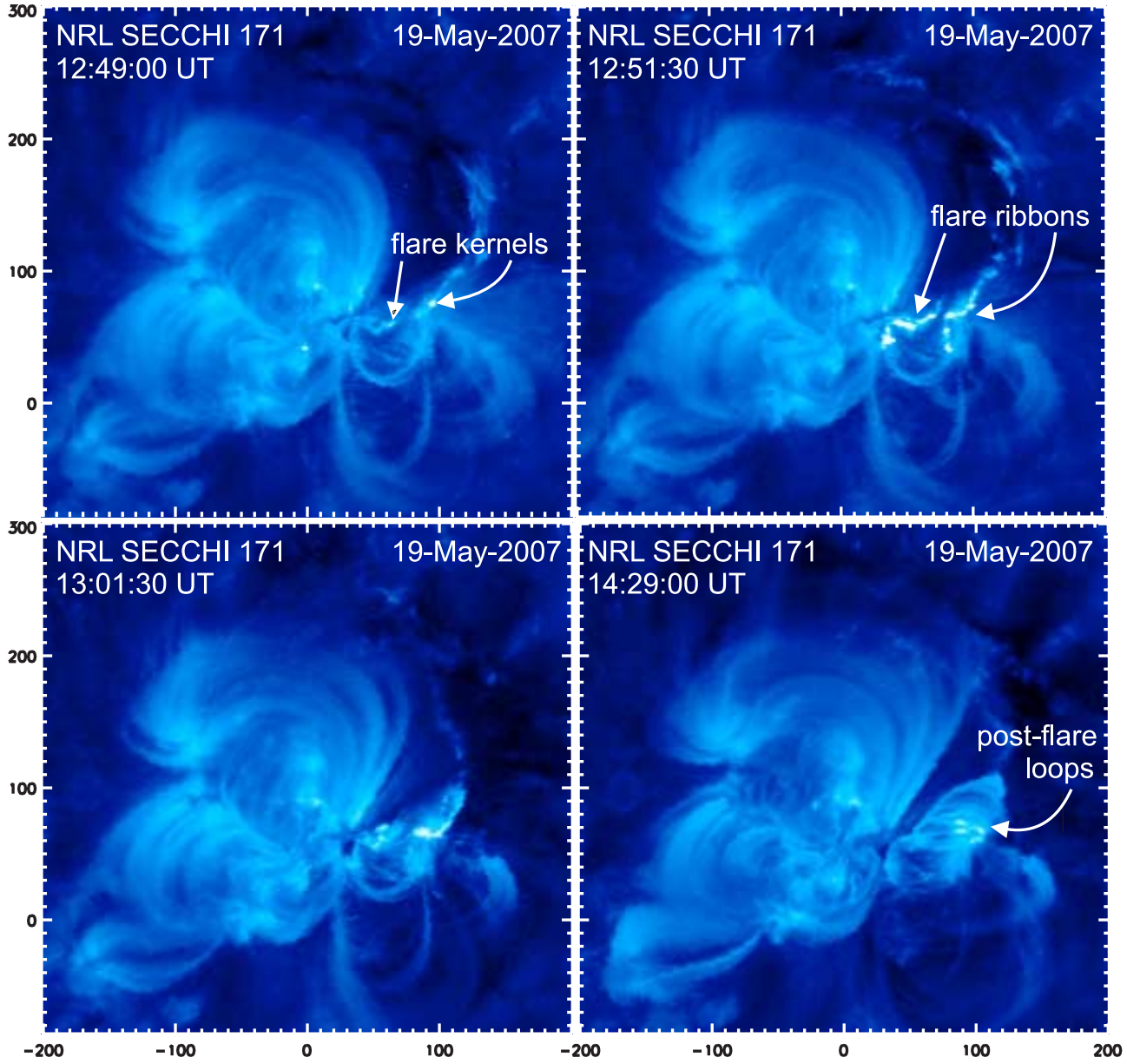

Figure 10. Evolution of the flare as seen in STEREO-A/EUVI 171 Å.

together to form a single low-noise magnetogram, which was used for further analysis.

[42] The determination of the magnetic flux

$$\varphi = \int B_n \cdot da, \tag{4}$$

which is reconnected during the flare, requires the measurement of the newly brightened flare area da at each time t, as well as the normal component of the magnetic field B_n inside this area. In order to be counted as a member of da, a particular pixel has to: (1) exceed a certain intensity threshold; (2) be a nonflare pixel in the preceding images; (3) exceed the MDI noise level of ±20 G; (4) be located inside the currently analyzed magnetic polarity, as the analysis has to be carried out separately for each magnetic polarity domain (for further detail, confer to *Miklenic et al.* [2007]). Taking the products of pixel area and B_n for each pixel inside the newly brightened area and adding them up yields the newly reconnected flux at each time t. Adding this flux to the flux that has been reconnected up to time t gives the cumulated magnetic reconnection flux at each time, i.e., a cumulated flux profile. Since equal amounts of positive and negative magnetic flux are involved in the reconnection process at each time, the profiles derived from the positive and negative polarity domains, $\varphi_+(t)$ and $\varphi_-(t)$, respectively, should be identical in the ideal case. The cumulated reconnection-flux profile $\varphi_r(t)$ is then calculated by taking the mean of both polarities:

$$\varphi_r(t) = \frac{\varphi_+(t) + |\varphi_-(t)|}{2}. \tag{5}$$

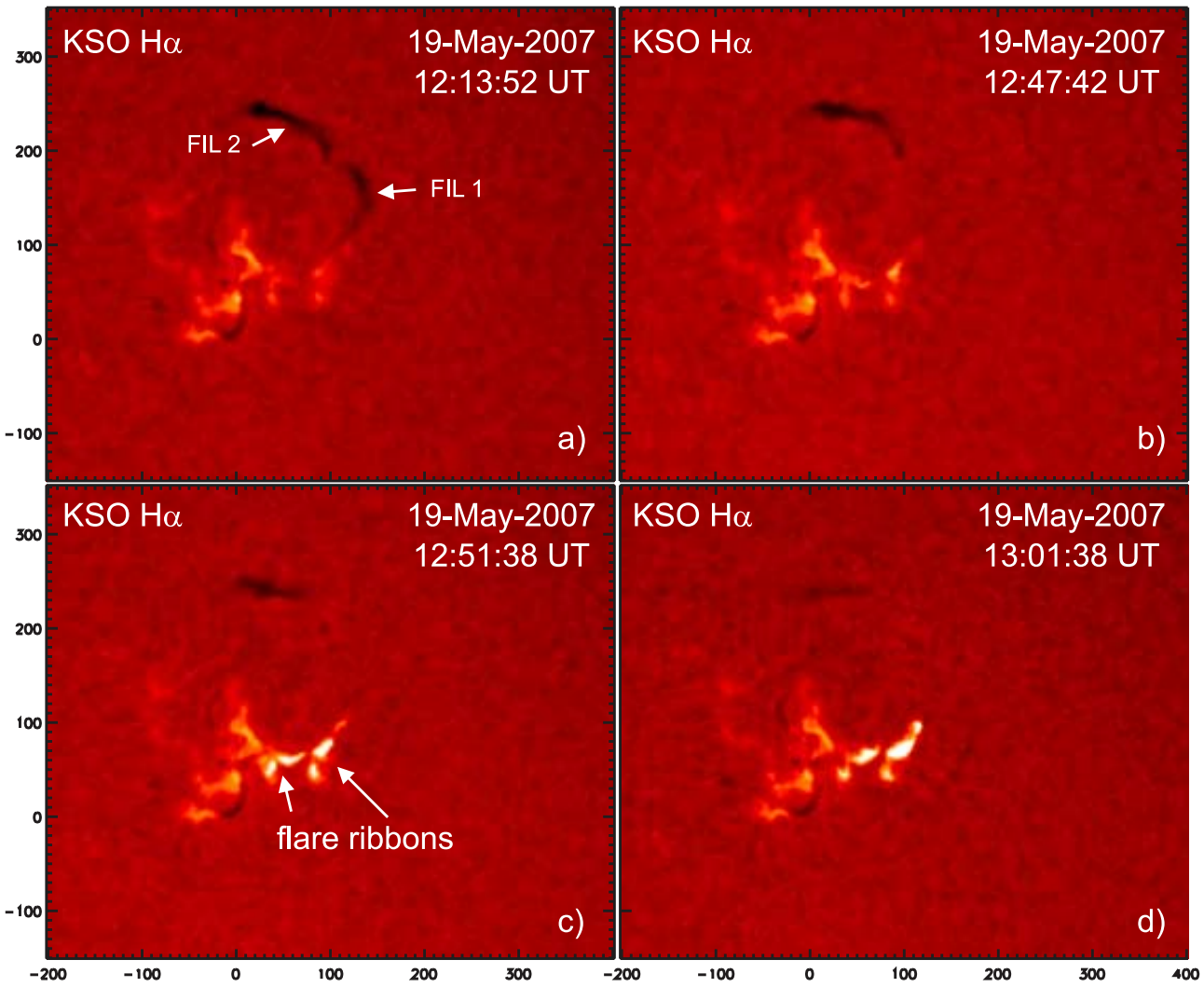

Figure 11. (a) Snapshot taken about 30 min before flare onset. Two erupting filaments (FIL 1, FIL 2) are visible at the top. (b) Situation directly before the flare: FIL 1 has left the Hα filter. (c) Impulsive phase: two bright flare ribbons appear and separate from each other. (d) Time of GOES maximum: FIL 2 has almost vanished from the Hα filter. – FOV: 600″ × 500″.

[43] Figure 12a shows the total area swept by the flare ribbons during the course of the event, which is the sum of all newly brightened areas. In Figure 12b the area contours are plotted on the MDI magnetogram. The size of the positive and negative-polarity areas is comparable. Both areas are elongated structures.

[44] Figure 13 shows that more negative than positive reconnection flux is detected. During the impulsive phase, when more and more flux is reconnected, the cumulated flux profiles steeply rise. In the decay phase, i.e., after the GOES X-ray flux reached its maximum, the reconnection process slowly comes to an end, and the amount of newly reconnected flux decreases. This results in nearly constant cumulated flux profiles during this phase of the event. At the end of the analyzed time interval the ratio of cumulated positive vs. negative flux is 0.64. The total flux adds up to 1.8×10^{21} Mx. Note that the Hα images were saturated, so the calculated flux is most likely overestimated (for details, see *Miklenic et al.* [2007]). The error estimate profiles were obtained, using upper and lower cutoff intensity thresholds for flare area detection.

4.2. Erupting Filament and CME Observations

[45] From Hα observations as shown in Figure 11 it is derived that the 19 May flare event is related with the eruption of two filaments, each associated to a separate CME [*Veronig et al.*, 2008]. The southern filament (FIL1) which is directly associated to the flaring region erupts to the west and is connected through timing and position to CME1 [*Veronig et al.*, 2008]. CME1 has a position angle of 271 degrees and an average speed of 960km/s in the LASCO field of view (LASCO CME catalogue, http://cdaw.gsfc.nasa.gov/CME_list). In comparison, FIL2 can be connected to CME2 moving in the northwestern direction with a position angle of 308 degrees and a mean velocity of 290 km/s, which is decelerating already in the LASCO field of view (Figure 14). The magnetic cloud observed at 1 AU ~58h later (GOES SXR peak: 19 May 13:00 UT, cloud front at WIND: 21 May 22:45 UT), has a

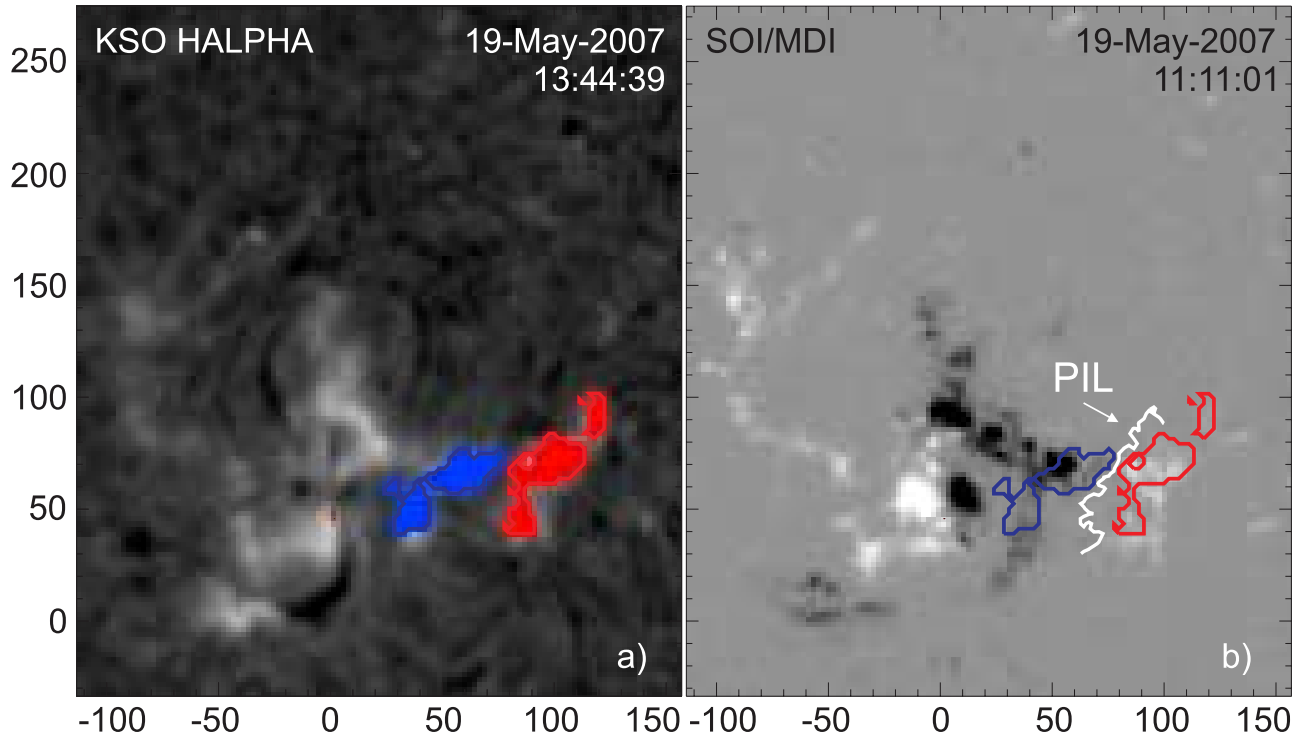

Figure 12. (a) Calculated total flare area on Hα image. Blue/red, negative/positive polarity. (b) Total flare area contours on MDI magnetogram; contour colors are the same as in Figure 12a; white line, magnetic polarity inversion line. MDI data range scaled to ±1000 G out of [−1900, 1910] G. – FOV: 268″ × 306″.

V_{HT} velocity of ∼450 km/s (see Table 1). It becomes obvious that only FIL1/CME1 with its speed profile can be attributed through the right timing to the MC of 22 May 2007.

[46] Focusing on FIL1 and assuming that the sheared arcade connected with the flare ribbons developed into the MC (see section 5.2), we obtain the magnetic orientation of the erupting flux rope as follows. In Figures 15 and 16, STEREO-A/EUVI images were corrected to Earth view and coaligned with the MDI magnetogram (Figure 15, bottom). Then, (1) the leading poloidal field is derived from the underlying magnetic field provided by the MDI instrument [*Scherrer et al.*, 1995] on board the Solar and Heliospheric Observatory (SOHO) (white arrow in Figure 15, bottom). (2) The direction of the axial field follows from the shearing direction of the associated initial flare brightenings, observed in EUV, with respect to the neutral line (see also Figure 16). The orientation of the axial magnetic field of the sheared arcade and the axial magnetic field of the MC with respect to the solar equator are given as yellow arrows in Figure 15. From this we derive that the erupting flux rope is right-handed on the Sun which is consistent with the handedness of the MC at 1 AU.

5. Discussion

5.1. Magnetic Cloud Shape

[47] In this particular event, observed by three spacecraft at different impact parameters, the aspect ratio derived from

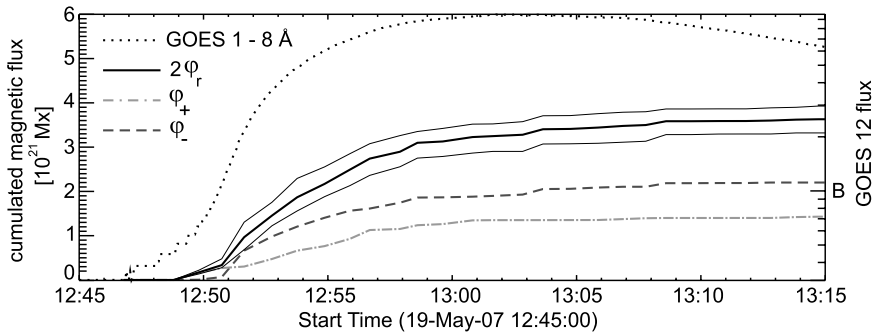

Figure 13. GOES12 1–8 Å soft X-ray profile, cumulated total magnetic reconnection flux (for the purpose of clarity we plot 2 φ_r) plus error estimate, derived from upper and lower cutoff intensity thresholds, and cumulated positive and negative reconnection flux (φ_+, φ_-).

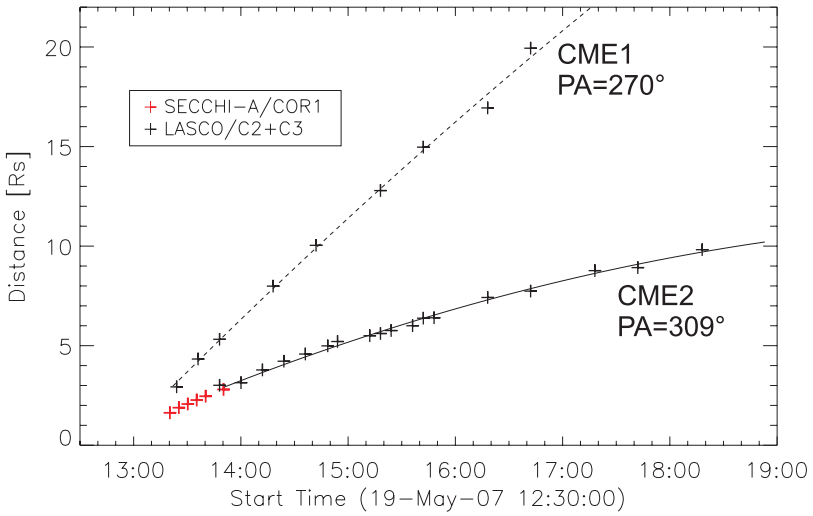

Figure 14. Kinematics of the CMEs associated with the event. CME1 was observed by LASCO C2 and C3; CME2 could as well be observed in the inner corona by STEREO COR1 (red pluses); the quadratic fit is given as dashed and solid black line for CME1 and CME2, respectively.

these observations (∼1.3:1) is much less than previously suggested by other studies. *Riley and Crooker* [2004] estimate from a kinematic treatment in a uniform solar wind that the MC cross section should have an aspect ratio of ∼5:1 or more, as also suggested by numerical simulations [e.g., *Manchester et al.*, 2004] and observations by ACE and Ulysses [*Liu et al.*, 2006]. For such high ratios, the cross section should look more like an arc or a "pancake" with a meridional component which is not negligible. The noncircular cross section was also suggested by studies on the CME acceleration and the aspect ratio enters into calculations of CME transit times; see review by *Forbes et al.* [2006]. However, the low aspect ratio of this particular MC implies that single-spacecraft cylindrical models can be quite successful in estimating magnetic fluxes and orientations for this event, which is indeed the case (see Table 1).

[48] An MCs shape may depend strongly on the solar wind environment through interactions with other ICMEs, high-speed streams or the heliospheric current sheet. This raises the question: Can the only slightly elongated shape of the 22 May 2007 cloud be explained by features in the ambient solar wind? The MC is situated inside slow solar wind (∼400 km/s) bracketed by two high-speed streams from two coronal holes to the east and west, respectively, of the active region from which the MC originated [*Kilpua et al.*, 2009; *Li et al.*, 2008]. Thus the MC was in the rarefaction region of the preceding high-speed stream from the western coronal hole. We speculate that this might be responsible for the cloud's low aspect ratio, as the solar wind pressure in which the cloud is running into is less than that compared to normal solar wind conditions. The trailing high speed stream from the eastern coronal hole may not have strongly interacted with the MC before 1 AU and thus influenced the shape, because this interaction was under development as the shock in the MCs rear part ran into the cloud between WIND and STEREO-B.

5.2. Origin of the MC From Magnetic Reconnection

[49] The magnetic fluxes of the magnetic cloud are Φ_p = 1.24×10^{21} Mx per AU and $\Phi_t = 0.4 \pm 0.1 \times 10^{21}$ Mx. The flare reconnected flux is $\varphi_r = 1.8 \times 10^{21}$ Mx. In Figure 8 these values are plotted with error bars additionally to the cumulated magnetic fluxes in the MC. The ratio $\Phi_p/\varphi_r \approx 1$ is consistent with the standard flare model but due to the large error bars arising from the incomplete observations, no definitive statement can be drawn between the preexisting and in situ models of CME initiation. Within the 2-D standard flare model, the axial flux cannot be described. To do this, a 3-D and finite sheared arcade model was developed by *Longcope and Beveridge* [2007] (hereinafter referred to as LB07), predicting a relation between the axial flux in the magnetic cloud and the ribbon flux

$$\Phi_{t;LB} = 0.1148 \times \varphi_r \tag{6}$$

for a shear of $S = 0.8$. In the framework of the LB07 model the value 0.1148 follows from the ratio of half of the total reconnected flux $2.09/2 \times \psi_0$ associated with the flare ribbons (this corresponds to our φ_r) and the axial flux $0.12 \times \psi_0$ in the ejected flux rope (see also Table 1 in the work of LB07; ψ_0 is a value connected to the photospheric flux in the LB07 model). S is the ratio of the relative displacement of the flare ribbons along the polarity inversion line (PIL) to the separation distance between negative and positive domains perpendicular to the PIL. We define the shearing angle δ to be the angle between a line perpendicular to the PIL and the line joining the initial flare kernels, and thus $S = \tan(\delta)$; see Figure 16. In our case, the result is $\delta = 50-60°$ and $S = 1.19-1.73$ with S = 1.43 for $\delta = 55°$. Unfortunately, this is a factor of 1.5–2 higher than the largest value $S = 0.8$ described in the LB07 model, so a direct comparison is not possible. We can, however, bring forward a plausibility argument: the comparison of $\Phi_{t;LB}$ = 0.2 ($S = 0.8$) to $\Phi_t = 0.4 \pm 0.1$ ($S = 1.43$) yields the conclusion

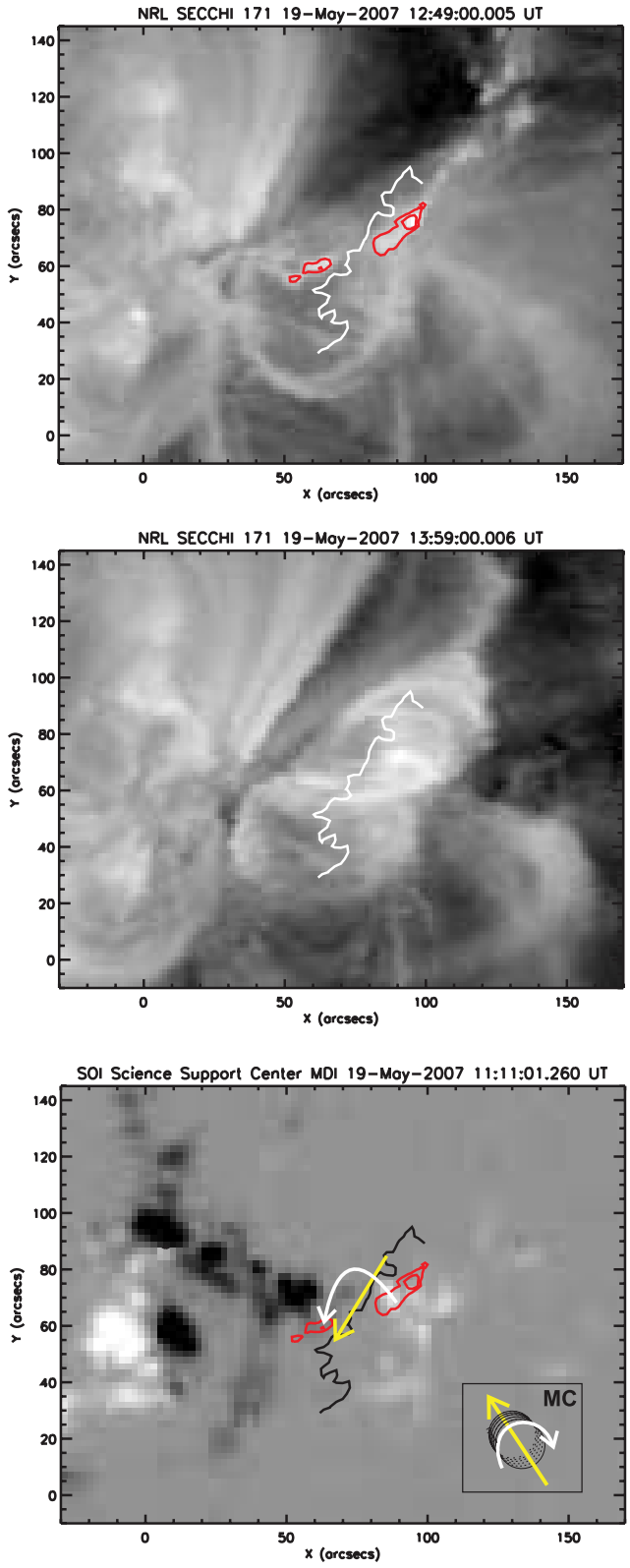

that at least half of the MCs magnetic flux has been added through reconnection during the eruption. Because $\Phi_{t;LB}$ is a monotonically increasing function of S (Figure 11 in the work of LB07) it is very likely that more than half of the clouds magnetic flux is formed in situ during the eruption. In any case, an extension of the LB model to $S \approx 1.5$ would be desirable to resolve this issue. We also note if at least half of the clouds flux was formed in situ, the poloidal flux should be $\varphi_r < \Phi_p < 2\varphi_r$ and $1.27 < L < 2.53$ AU, which are reasonable values. (See discussions in the works of *Leamon et al.* [2004] and *Qiu et al.* [2007].)

5.3. Rotation of the Cloud Axis

[50] The magnetic cloud axis at 1 AU and the orientation of the polarity inversion line (PIL) differ by about 100 degrees as can be seen from Figure 15. FIL1 is curved (Figure 11) but the PIL is almost straight (Figure 16). We work with the hypothesis that the orientation of the plasmoid formed during the eruption is mainly determined by the PIL between the flare ribbons because at least half of the MCs flux (and likely more) is created during the eruption. We define an angle α in a plane perpendicular to the Sun-Earth line measured clockwise from solar east with respect to the solar equator. The axial field of the erupting plasmoid on the Sun points to $\alpha_{SUN} = 305°$, and the MCs axial field to $\alpha_{MC} = 55°$. The difference is $\approx 110°$ for a clockwise rotation.

[51] The amount of rotation and its direction is consistent with the helical kink instability [e.g., *Fan and Gibson*, 2003; *Rust and LaBonte*, 2005; *Green et al.*, 2007]. The clockwise rotation is expected for a right-handed flux rope and the rotation angle of 110° is close to the values seen in the numerical simulation of *Fan and Gibson* [2003] and events reported by *Rust et al.* [2005]. Because CME1 was too faint (see section 4.2), it could not be fitted to an ellipse from which the CME orientation angle can be determined [*Yurchyshyn et al.*, 2007]. Thus it is unclear if the rotation took place already in the solar corona or farther out in the heliosphere.

[52] It is interesting to note that the eruption was situated right under the heliospheric current sheet [*Li et al.*, 2008; *Kilpua et al.*, 2009]. *Yurchyshyn* [2008] found for 25 events a very good correlation between the MC axis orientation at 1 AU and the inclination of the heliospheric current sheet, approximated by the coronal neutral line (CNL) in synoptic coronal magnetic field maps by the Wilcox Solar observa-

Figure 15. (top) STEREO-A/EUVI 171 Å image of the earliest flare kernels, overlaid with contour lines of the first brightenings (red line) before the impulsive flaring phase started and the neutral line (white line) as derived from the corresponding magnetogram (Figure 15, bottom). (middle) STEREO-A/EUVI 171 Å image showing postflare loops, overlaid with the magnetic neutral line for orientation. (bottom) MDI line-of-sight magnetogram of the active region (white, positive polarity; black, negative polarity). White and yellow arrows indicate the leading poloidal and the axial field direction, respectively. The inlay in the right corner shows the leading poloidal and the axial field direction of the flux rope observed at 1 AU (orientation of the MC axial field with respect to the solar equator).

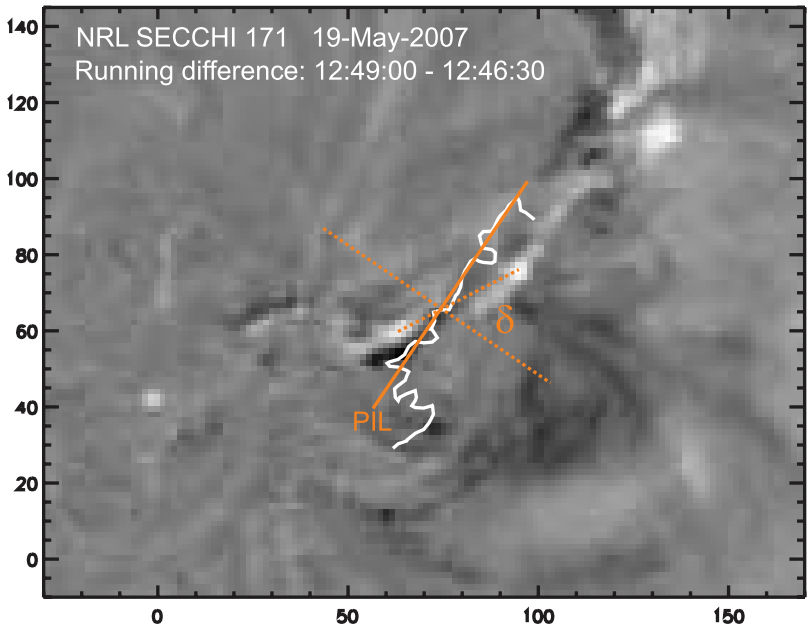

Figure 16. Determination of the shearing angle δ from a STEREO-A/EUVI 171 Å difference image. The polarity inversion line (PIL, white) is well approximated by a straight line (orange) between the initial flare brightenings, connected by an orange dotted line. Angle δ is measured between a line perpendicular to the PIL (also orange dotted) and the line joining the initial flare kernels, yielding $\delta = 55° \pm 5$ and shear parameter $S = 1.20–1.73$ (see text).

tory [*Hoeksema et al.*, 1983]. In the view of this the 22 May 2007 MC event is rather unusual as there is a difference of ≈60° between the MC inclination α_{MC} = 55° and the CNL inclination $\alpha_{CNL} \approx 115°$ inferred from the classic Wilcox Solar observatory map for Carrington rotation 2056 (Figure 17). However, the active region is situated exactly under the CNL and its highly nonpotential field may significantly distort its structure, an effect which is not accounted for by the potential field model.

[53] In summary, it seems plausible that a right-handed flux rope with axial field pointing southward erupted, rotated clockwise through the helical kink instability and arrived at Earth with a northward pointing axial field

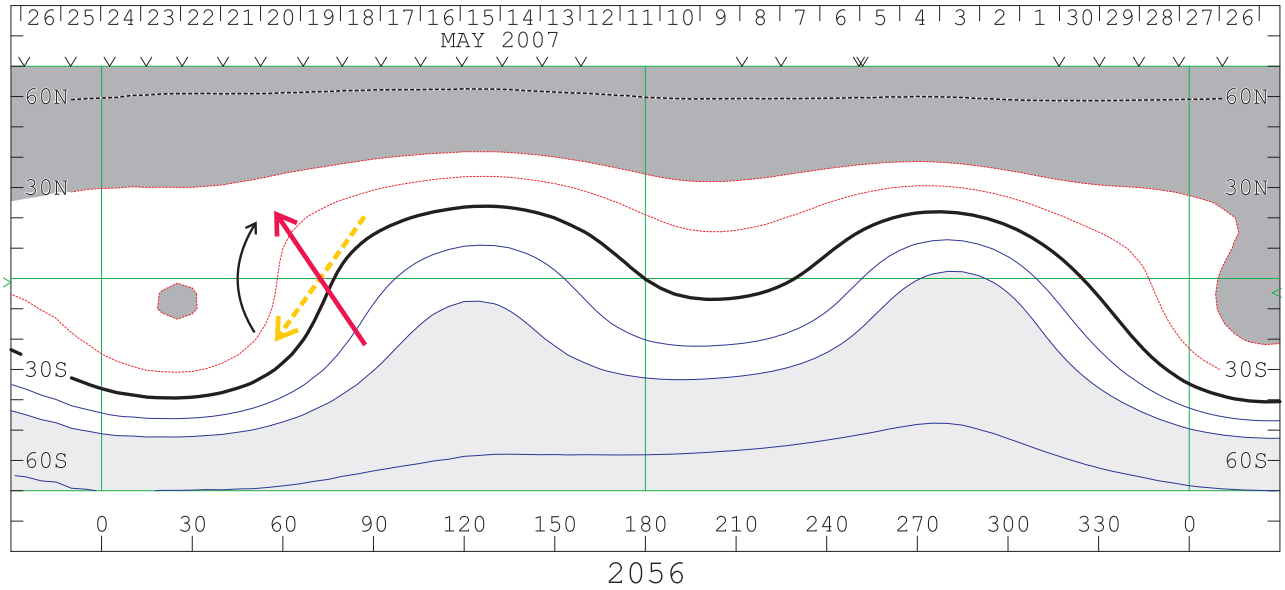

Figure 17. Synoptic coronal magnetic field map from the Wilcox Solar observatory (classic). The thick black line indicates the coronal neutral line. Red arrow, MC orientation at 1 AU with respect to the solar equator. Yellow arrow, orientation of the polarity inversion line and the axial field of the erupting flux rope (same as in Figure 15, bottom).

making it completely nongeoeffective which is consistent with the in situ observations.

6. Summary and Conclusions

[54] In this paper we applied for the first time a Grad-Shafranov technique combining observations by two spacecraft which are separated by a distance of 0.06 AU, i.e., one of the same order of magnitude as the radial diameter of the magnetic cloud (0.19 AU). This procedure was introduced earlier in the magnetospheric context [*Sonnerup et al.*, 2004; *Hasegawa et al.*, 2006]. Through creating a magnetic field map at one spacecraft and correlating its predictions with the observations by the other spacecraft we inferred that the method assumptions of invariance and time independence are valid. These field maps were then merged into a single combined magnetic field map (Figure 4), which shows MC core field lines possessing a close-to-circular shape, demonstrated by the observations at WIND displaced at a distance, perpendicular to the MC axis, of 50% of the cloud's half radial diameter (0.095 AU). Observations by STEREO-A, passing at a thus defined impact parameter of 140% show a much shorter interval of similarly rotating field lines indicating the flank of the MC. These measurements point to elongated and ''flattened'' field lines in the outer part of the MC but they could not be included in the present technique probably because of strong interaction of the MC flank with the surrounding solar wind. The circular (force-free) shape of the MC core field lines could be a consequence of the strong internal axial field compared to the weaker azimuthal field and elongated outer field lines.

[55] This particular event took place almost at solar minimum in a solar wind environment which is dominated by solar wind streams varying largely in speed (300–800 km/s). This magnetic cloud was embedded between two fast streams in a V-like speed profile which is a rather unusual situation; for data plots surrounding the event, see *Kilpua et al.* [2009]. We suggest this particular configuration be examined by theorists and modelers alike in view of the less than expected elongated shape. The unique complementary measurements by STEREO-A/B and WIND for this event also allow to test the ability of other models to reproduce quantitatively the observations of all three spacecraft, especially the fitting technique using an elliptical cross section [*Hidalgo et al.*, 2002]. With these observations it should be possible to constrain the set of free parameters used in these kind of models.

[56] Taking advantage of multispacecraft information we were able to investigate closer the relation between the magnetic clouds in situ signature and its solar counterparts. Thus the second main conclusion is that magnetic reconnection is highly relevant for CME initiation models and the origin of magnetic clouds. With a good coverage of the magnetic cloud's cross section by three spacecraft we were able to obtain a robust axial flux. This was compared with the predicted relation between the flare reconnected flux (inferred from flare ribbon observations) and the axial flux of the ejected plasmoid in the 3-D finite sheared arcade model by *Longcope and Beveridge* [2007]. We found values of the shear which were outside the range of those in the model, but from a plausibility argument it follows that at least half of the MCs magnetic flux was created in situ during the eruption. This is consistent with case studies finding an agreement between the flare ribbon flux and MC fluxes [*Longcope et al.*, 2007; *Möstl et al.*, 2008] and the statistical study by *Qiu et al.* [2007]. In this respect we also point out the finding of *Leamon et al.* [2004] that the twist in MCs far exceeds the twist from linear force-free modeled active region magnetic fields, so that a large amount of twist should be added during the eruption through reconnection.

[57] Our results support the impulsive formation of a helical flux rope from a sheared arcade configuration [e.g., *Démoulin et al.*, 1996; *Longcope et al.*, 2007], but they do not completely rule out a preexisting flux rope. To settle this issue an extension of the *Longcope et al.* [2007] model to larger shear parameters would be needed. However, there are clear indications of a preexisting structure surrounding the flare polarity inversion line before the eruption, such as the filament and a sigmoid seen in X-ray observations by Hinode/XRT [*Li et al.*, 2008]. At the present state of the art, it seems that none of the two models can alone explain consistently the observations both on the Sun and at 1 AU; we need elements of both. *Lin et al.* [2004] present a model where a preexisting flux rope doubles its flux during eruption through reconnection in its wake, and *Amari et al.* [2000] present a 3-D simulation of such a process. Thus rather than clearly drawing a line between the preexisting and in situ models we raise the question: which process is more relevant in defining the structure reaching 1 AU? Our results that less than half of the MCs axial flux is preexisting suggests that the eruption itself is very likely to be more important in determining the structure of the ejected flux rope. In summary, the preexisting filament/sigmoid structure is likely to carry only a small amount of magnetic flux compared to the magnetic cloud at 1 AU. This is also supported by the study of *Qiu et al.* [2007], who reported no significant differences in flux budgets for events with or without a filament eruption.

[58] The promising results of *Yurchyshyn* [2008] show MC axes to be related to the coronal neutral line from a potential field model, which is an important finding for space weather forecasting purposes. For the 21–22 May 2007 magnetic cloud the predictive capability of this relation is rather poor. The reason might be that the active region is situated almost exactly under the coronal neutral line which in this case is not well represented by a potential field. At Earth, the MC is indeed embedded in the front of a larger scale structure resembling the heliospheric current sheet [*Kilpua et al.*, 2009]. We instead find the orientation of the MC consistent with the rotation of the erupting flux rope through the helical kink instability, assuming no significant rotation took place in the interplanetary medium. If the orientation of the MC at Earth is determined also through the helical kink instability, which factors decide the amount of rotation? The decay of the overlying field and its strength might determine the onset of a full eruption either through the kink or torus instabilities, at least in some events [*Liu*, 2008], while the amount of rotation is also different for those two instabilities [*Fan and Gibson*, 2007]. It is known that there are lots of events where the PIL and MC axis fit well for quiescent filament eruptions [e.g., *Bothmer and Schwenn*, 1998; *Zhao and Hoeksema*, 1998]. However, especially for those fast and geoeffective eruptions associated with active regions, events have been

observed with rotations up to 180 degrees [*Harra et al.*, 2007], posing a challenge for space weather forecasting efforts.

[59] **Acknowledgments.** C.M. is supported by the young researchers fund of the Steiermärkische Sparkasse. C.J.F. is a co-Investigator on STEREO/PLASTIC. This work is supported by NASA WIND/SWE and MFI grants NNG06GC75G, NNG06GD41G and NNX08AD11G. Work at the University of California, Berkeley, was supported from STEREO grant NAS5-03131. It is also supported by the Austrian Fonds zur Förderung der wissenschaftlichen Forschung under projects P20145-N16 and P20131-N16. M. Temmer acknowledges project APART 11262 of the Austrian Academy of Sciences. We also acknowledge the use of WIND data provided by the magnetometer and the solar wind experiment teams at GSFC. This research was supported in part by an appointment to the NASA Postdoctoral Program at Goddard Space Flight Center, administered by Oak Ridge Associated Universities through a contract with NASA.

[60] Zuyin Pu thanks M. A. Hidalgo and another reviewer for their assistance in evaluating this paper.

References

Acuña, M. H., D. Curtis, J. L. Scheifele, C. T. Russell, P. Schroeder, A. Szabo, and J. G. Luhmann (2007), The STEREO/IMPACT magnetic field experiment, *Space Sci. Rev.*, *208*, doi:10.1007/s11214-007-9259-2.

Amari, T., J. F. Luciani, Z. Mikic, and J. Linker (2000), A twisted flux rope model for coronal mass ejections and two-ribbon flares, *Astrophys. J.*, *529*, L49–L52, doi:10.1086/312444.

Antiochos, S. K., C. R. DeVore, and J. A. Klimchuk (1999), A model for solar coronal mass ejections, *Astrophys. J.*, *510*, 485–493, doi:10.1086/306563.

Bothmer, V., and R. Schwenn (1998), The structure and origin of magnetic clouds in the solar wind, *Ann. Geophys.*, *16*, 1–24.

Burlaga, L. F. (1988), Magnetic clouds and force-free fields with constant alpha, *J. Geophys. Res.*, *93*, 7217–7224.

Burlaga, L., E. Sittler, F. Mariani, and R. Schwenn (1981), Magnetic loop behind an interplanetary shock - Voyager, Helios, and IMP 8 observations, *J. Geophys. Res.*, *86*, 6673–6684.

Chen, J. (1989), Effects of toroidal forces in current loops embedded in a background plasma, *Astrophys. J.*, *338*, 453–470, doi:10.1086/167211.

Démoulin, P., E. R. Priest, and D. P. Lonie (1996), Three-dimensional magnetic reconnection without null points: 2. Application to twisted flux tubes, *J. Geophys. Res.*, *101*, 7631–7646, doi:10.1029/95JA03558.

Fan, Y., and S. E. Gibson (2003), The emergence of a twisted magnetic flux tube into a preexisting coronal arcade, *Astrophys. J.*, *589*, L105–L108, doi:10.1086/375834.

Fan, Y., and S. E. Gibson (2007), Onset of coronal mass ejections due to loss of confinement of coronal flux ropes, *Astrophys. J.*, *668*, 1232–1245, doi:10.1086/521335.

Farrugia, C. J., L. F. Burlaga, V. A. Osherovich, I. G. Richardson, M. P. Freeman, R. P. Lepping, and A. J. Lazarus (1993), A study of an expanding interplanatary magnetic cloud and its interaction with the Earth's magnetosphere: The interplanetary aspect, *J. Geophys. Res.*, *98*, 7621–7632.

Forbes, T. G., et al. (2006), CME theory and models, *Space Sci. Rev.*, *123*, 251–302, doi:10.1007/s11214-006-9019-8.

Galvin, A. B., et al. (2008), The Plasma and Suprathermal Ion Composition (PLASTIC) investigation on the STEREO observatories, *Space Sci. Rev.*, *136*, 437, doi:10.1007/s11214-007-9296-x.

Green, L. M., B. Kliem, T. Török, L. van Driel-Gesztelyi, and G. D. R. Attrill (2007), Transient coronal sigmoids and rotating erupting flux ropes, *Sol. Phys.*, *246*, 365–391, doi:10.1007/s11207-007-9061-z.

Gulisano, A. M., S. Dasso, C. H. Mandrini, and P. Démoulin (2007), Estimation of the bias of the minimum variance technique in the determination of magnetic clouds global quantities and orientation, *Adv. Space Res.*, *40*, 1881–1890, doi:10.1016/j.asr.2007.09.001.

Harra, L. K., et al. (2007), How does large flaring activity from the same active region produce oppositely directed magnetic clouds?, *Sol. Phys.*, *244*, 95–114, doi:10.1007/s11207-007-9002-x.

Hasegawa, H., B. U. Ö. Sonnerup, B. Klecker, G. Paschmann, M. W. Dunlop, and H. Rème (2005), Optimal reconstruction of magnetopause structures from Cluster data, *Ann. Geophys.*, *23*, 973–982.

Hasegawa, H., B. U. Ö. Sonnerup, C. J. Owen, B. Klecker, G. Paschmann, A. Balogh, and H. Rème (2006), The structure of flux transfer events recovered from Cluster data, *Ann. Geophys.*, *24*, 603–618.

Hasegawa, H., B. U. Ö. Sonnerup, M. Fujimoto, Y. Saito, and T. Mukai (2007), Recovery of streamlines in the flank low-latitude boundary layer, *J. Geophys. Res.*, *112*, A04213, doi:10.1029/2006JA012101.

Hau, L.-N., and B. U. Ö. Sonnerup (1999), Two-dimensional coherent structures in the magnetopause: Recovery of static equilibria from single-spacecraft data, *J. Geophys. Res.*, *104*, 6899–6918, doi:10.1029/1999JA900002.

Hidalgo, M. A. (2003), A study of the expansion and distortion of the cross section of magnetic clouds in the interplanetary medium, *J. Geophys. Res.*, *108*(A8), 1320, doi:10.1029/2002JA009818.

Hidalgo, M. A., T. Nieves-Chinchilla, and C. Cid (2002), Elliptical cross-section model for the magnetic topology of magnetic clouds, *Geophys. Res. Lett.*, *29*(13), 1637, doi:10.1029/2001GL013875.

Hoeksema, J. T., J. M. Wilcox, and P. H. Scherrer (1983), The structure of the heliospheric current sheet: 1978–1982, *J. Geophys. Res.*, *88*, 9910–9918.

Hu, Q., and B. U. Ö. Sonnerup (2002), Reconstruction of magnetic clouds in the solar wind: Orientations and configurations, *J. Geophys. Res.*, *107*(A7), 1142, doi:10.1029/2001JA000293.

Hu, Q., C. W. Smith, N. F. Ness, and R. M. Skoug (2004), Multiple flux rope magnetic ejecta in the solar wind, *J. Geophys. Res.*, *109*, A03102, doi:10.1029/2003JA010101.

Hu, Q., C. W. Smith, N. F. Ness, and R. M. Skoug (2005), On the magnetic topology of October/November 2003 events, *J. Geophys. Res.*, *110*, A09S03, doi:10.1029/2004JA010886.

Huttunen, K. E. J., R. Schwenn, V. Bothmer, and H. E. J. Koskinen (2005), Properties and geoeffectiveness of magnetic clouds in the rising, maximum and early declining phases of solar cycle 23, *Ann. Geophys.*, *23*, 625–641.

Khrabrov, A. V., and B. U. Ö. Sonnerup (1998), deHoffmann-Teller analysis, in *Analysis Methods for Multi-Spacecraft Data*, edited by G. Paschmann and P. W. Daly, *ESA SR-001*, p. 221, Eur. Space Agency, Noordwijk, Netherlands.

Kilpua, E. K. J., et al. (2009), Multispacecraft observations of magnetic clouds and their solar origins May 19–23, 2007, *Sol. Phys.*, in press.

Klein, L. W., and L. F. Burlaga (1982), Interplanetary magnetic clouds at 1 AU, *J. Geophys. Res.*, *87*, 613–624, doi:10.1029/JA087iA02p00613.

Leamon, R. J., R. C. Canfield, S. L. Jones, K. Lambkin, B. J. Lundberg, and A. A. Pevtsov (2004), Helicity of magnetic clouds and their associated active regions, *J. Geophys. Res.*, *109*, A05106, doi:10.1029/2003JA010324.

Leitner, M., C. J. Farrugia, C. Möstl, K. W. Ogilvie, A. B. Galvin, R. Schwenn, and H. K. Biernat (2007), Consequences of the force-free model of magnetic clouds for their heliospheric evolution, *J. Geophys. Res.*, *112*, A06113, doi:10.1029/2006JA011940.

Lepping, R. P., L. F. Burlaga, and J. A. Jones (1990), Magnetic field structure of interplanetary magnetic clouds at 1 AU, *J. Geophys. Res.*, *95*, 11,957–11,965.

Lepping, R. P., et al. (1995), The wind magnetic field investigation, *Space Sci. Rev.*, *71*, 207–229.

Li, Y., B. J. Lynch, G. Stenborg, J. G. Luhmann, K. E. J. Huttunen, B. T. Welsch, P. C. Liewer, and A. Vourlidas (2008), The solar magnetic field and coronal dynamics of the eruption on 2007 May 19, *Astrophys. J.*, *681*, L37–L40, doi:10.1086/590340.

Lin, J., J. C. Raymond, and A. A. van Ballegooijen (2004), The role of magnetic reconnection in the observable features of solar eruptions, *Astrophys. J.*, *602*(1), 422–435.

Liu, Y. (2008), Magnetic field overlying solar eruption regions and kink and torus instabilities, *Astrophys. J.*, *679*, L151–L154, doi:10.1086/589282.

Liu, Y., J. D. Richardson, J. W. Belcher, C. Wang, Q. Hu, and J. C. Kasper (2006), Constraints on the global structure of magnetic clouds: Transverse size and curvature, *J. Geophys. Res.*, *111*, A12S03, doi:10.1029/2006JA011890.

Liu, Y., J. G. Luhmann, K. E. J. Huttunen, R. P. Lin, S. D. Bale, C. T. Russell, and A. B. Galvin (2008), Reconstruction of the 2007 May 22 magnetic cloud: How much can we trust the flux-rope geometry of CMEs?, *Astrophys. J.*, *677*, L133–L136, doi:10.1086/587839.

Longcope, D. W., and C. Beveridge (2007), A quantitative, topological model of reconnection and flux rope formation in a two-ribbon flare, *Astrophys. J.*, *669*, 621–635.

Longcope, D., C. Beveridge, J. Qiu, B. Ravindra, G. Barnes, and S. Dasso (2007), Modeling and measuring the flux reconnected and ejected by the two-ribbon flare/CME event on 7 November 2004, *Sol. Phys.*, *81*, doi:10.1007/s11207-007-0330-7.

Luhmann, J. G., et al. (2008), STEREO IMPACT investigation goals, measurements, and data products overview, *Space Sci. Rev.*, *136*, 117–184, doi:10.1007/s11214-007-9170-x.

Lynch, B. J., J. R. Gruesbeck, T. H. Zurbuchen, and S. K. Antiochos (2005), Solar cycle-dependent helicity transport by magnetic clouds, *J. Geophys. Res.*, *110*, A08107, doi:10.1029/2005JA011137.

Manchester, W. B., T. I. Gombosi, I. Roussev, D. L. De Zeeuw, I. V. Sokolov, K. G. Powell, G. Tóth, and M. Opher (2004), Three-dimen-

sional MHD simulation of a flux rope driven CME, *J. Geophys. Res.*, *109*, A01102, doi:10.1029/2002JA009672.

Marubashi, K., and R. P. Lepping (2007), Long-duration magnetic clouds: A comparison of analyses using torus- and cylinder-shaped flux rope models, *Ann. Geophys.*, *25*, 2453–2477.

Miklenic, C. H., A. M. Veronig, B. Vršnak, and A. Hanslmeier (2007), Reconnection and energy release rates in a two-ribbon flare, *Astron. Astrophys.*, *461*, 697–706, doi:10.1051/0004-6361:20065751.

Moore, R. L., and B. J. Labonte (1980), The filament eruption in the 3B flare of July 29, 1973: Onset and magnetic field configuration, in *Solar and Interplanetary Dynamics, Proceedings of IAU Symposium*, vol. 91, edited by M. Dryer and E. Tandberg-Hanssen, pp. 207–210, D. Reidel, Dordrecht, Netherlands.

Möstl, C., C. Miklenic, C. J. Farrugia, M. Temmer, A. Veronig, A. B. Galvin, B. Vršnak, and H. K. Biernat (2008), Two-spacecraft reconstruction of a magnetic cloud and comparison to its solar source, *Ann. Geophys.*, *26*, 3139–3152.

Ogilvie, K. W., et al. (1995), SWE: A comprehensive plasma instrument for the Wind spacecraft, *Space Sci. Rev.*, *71*, 55–77.

Otruba, W., and W. Pötzi (2003), The new high-speed Hα imaging system at Kanzelhöhe Solar Observatory, *Hvar Obs. Bull.*, *27*, 189–195.

Owens, M. J., V. G. Merkin, and P. Riley (2006), A kinematically distorted flux rope model for magnetic clouds, *J. Geophys. Res.*, *111*, A03104, doi:10.1029/2005JA011460.

Qiu, J., Q. Hu, T. A. Howard, and V. B. Yurchyshyn (2007), On the magnetic flux budget in low-corona magnetic reconnection and interplanetary coronal mass ejections, *Astrophys. J.*, *659*(1), 758, doi:10.1086/512060.

Riley, P., and N. U. Crooker (2004), Kinematic treatment of coronal mass ejection evolution in the solar wind, *Astrophys. J.*, *600*, 1035–1042, doi:10.1086/379974.

Riley, P., et al. (2004), Fitting flux ropes to a global MHD solution: A comparison of techniques, *J. Atmos. Sol. Terr. Phys.*, *66*, 1321–1331, doi:10.1016/j.jastp.2004.03.019.

Romashets, E. P., and M. Vandas (2003), Force-free field inside a toroidal magnetic cloud, *Geophys. Res. Lett.*, *30*(20), 2065, doi:10.1029/2003GL017692.

Rust, D. M., and B. J. LaBonte (2005), Observational evidence of the kink instability in solar filament eruptions and sigmoids, *Astrophys. J.*, *622*, L69–L72, doi:10.1086/429379.

Rust, D. M., B. J. Anderson, M. D. Andrews, M. H. Acuña, C. T. Russell, P. W. Schuck, and T. Mulligan (2005), Comparison of interplanetary disturbances at the NEAR spacecraft with coronal mass ejections at the Sun, *Astrophys. J.*, *621*, 524–536, doi:10.1086/427401.

Scherrer, P. H., et al. (1995), The Solar Oscillations Investigation - Michelson Doppler Imager, *Sol. Phys.*, *162*, 129–188, doi:10.1007/BF00733429.

Sonnerup, B. U. O., and L. J. Cahill Jr. (1967), Magnetopause structure and attitude from Explorer 12 observations, *J. Geophys. Res.*, *72*, 171.

Sonnerup, B. U. Ö., H. Hasegawa, and G. Paschmann (2004), Anatomy of a flux transfer event seen by Cluster, *Geophys. Res. Lett.*, *31*, L11803, doi:10.1029/2004GL020134.

Sonnerup, B. U. Ö., H. Hasegawa, W.-L. Teh, and L.-N. Hau (2006), Grad-Shafranov reconstruction: An overview, *J. Geophys. Res.*, *111*, A09204, doi:10.1029/2006JA011717.

Sturrock, P. A. (1994), *Plasma Physics: An Introduction to the Theory of Astrophysical, Geophysical and Laboratory Plasmas*, Cambridge Univ. Press, New York.

Su, Y., A. Van Ballegooijen, J. McCaughey, E. Deluca, K. K. Reeves, and L. Golub (2007), What determines the intensity of solar flare/CME events?, *Astrophys. J.*, *665*, 1448–1459, doi:10.1086/519679.

van Ballegooijen, A. A., and P. C. H. Martens (1989), Formation and eruption of solar prominences, *Astrophys. J.*, *343*, 971–984, doi:10.1086/167766.

Veronig, A. M., M. Temmer, and B. Vršnak (2008), High-cadence observations of a global coronal wave by STEREO EUVI, *Astrophys. J.*, *681*, L113–L116, doi:10.1086/590493.

Yurchyshyn, V. (2008), Relationship between EIT posteruption arcades, coronal mass ejections, the coronal neutral line, and magnetic clouds, *Astrophys. J.*, *675*, L49–L52, doi:10.1086/533413.

Yurchyshyn, V., Q. Hu, R. P. Lepping, B. J. Lynch, and J. Krall (2007), Orientations of LASCO Halo CMEs and their connection to the flux rope structure of interplanetary CMEs, *Adv. Space Res.*, *40*, 1821–1826, doi:10.1016/j.asr.2007.01.059.

Zhao, X. P., and J. T. Hoeksema (1998), Central axial field direction in magnetic clouds and its relation to southward interplanetary magnetic field events and dependence on disappearing solar filaments, *J. Geophys. Res.*, *103*, 2077–2083.

H. K. Biernat, M. Temmer and A. Veronig, Institute of Physics, University of Graz, A-8010 Graz, Austria.

C. J. Farrugia and A. B. Galvin, Space Science Center and Department of Physics, University of New Hampshire, 39 College Road, Durham, NH 03824, USA. (charlie.farrugia@unh.edu)

E. K. J. Kilpua and J. G. Luhmann, Space Sciences Laboratory, University of California, Berkeley, CA 94720, USA.

M. Leitner, Institute for Astro- and Particle Physics, University of Innsbruck, A-6020 Innsbruck, Austria.

C. Miklenic and C. Möstl, Space Research Institute, Austrian Academy of Sciences, Schmiedlstrasse 6, A-8042 Graz, Austria. (moestlch@stud.uni-graz.at; christiane.miklenic@uni-graz.at)

T. Nieves-Chinchilla, Geospace Physics Laboratory, NASA Goddard Space Flight Center, Greenbelt, MD 20771, USA.